Interaction effects in the transport of particles in nanowire quantum dots

Kristinsdottir, Liney Halla

2015

INTERACTION EFFECTS IN THE TRANSPORT OF PARTICLES IN NANOWIRE QUANTUM DOTS

Líney Halla Kristinsdóttir

Division of Mathematical Physics
Faculty of Engineering
Lund University

THESIS FOR THE DEGREE OF
DOCTOR OF PHILOSOPHY IN ENGINEERING

Thesis advisor:
Stephanie M. Reimann

Faculty opponent:
Peter Schmelcher

Doctoral thesis which, by due permission from the Faculty of Engineering at Lund University, will be publicly defended in Lundamarksalen at Lund Observatory, Sölvegatan 27, Lund, on Tuesday, May 12, 2015, at 10:15, for the degree of Doctor of Philosophy in Engineering.

DOKUMENTDATABLAD enl SIS 61 41 21

Organization	Document name
LUND UNIVERSITY Division of Mathematical Physics Department of Physics Sölvegatan 14A SE–223 62 LUND Sweden	**DOCTORAL THESIS**
	Date of issue 2014-04-16
	Sponsoring organization
Author(s) Líney Halla Kristinsdóttir	

Title and subtitle

Interaction effects in the transport of particles in nanowire quantum dots

Abstract

Interactions between physical bodies constantly affect their properties. This thesis presents a theoretical study on the effects of interaction in few-body nanowire quantum dots. The focus is to a large extent on a phenomenon called Wigner localization, and how this, as well as other interaction effects, can be identified in an experiment by transport spectroscopy and by thermopower measurements. The physical systems considered are electrons in semiconductor nanowires and an ultracold gas of dipolar particles in magneto-optical traps. The full many-body description of the nanowire quantum dot is obtained by exact diagonalization (also known as the configuration interaction method) while the transport simulations are based on a Pauli master equation approach. The thesis is based on three papers: In Paper I we examine Wigner localization in an InSb nanowire quantum dot and identify the onset of Wigner localization in an experiment. In Paper II we study how different interaction regimes can be accessed in an ultracold dipolar gas by tuning the dipole-dipole interaction externally, providing Wigner localization for strong repulsion and total current blockade for attraction. The effect of excited states on the thermopower lineshape is investigated in Paper III, asserting the possibility to detect the onset of Wigner localization by thermopower measurements.

Key words:

Quantum dots, semiconductor nanowires, ultracold dipolar gases, electron transport, atom transport, Wigner localization, current blockade, thermopower

Classification system and/or index terms (if any):

Supplementary bibliographical information:	Language English
ISSN and key title:	ISBN 978-91-7623-279-8 (print) 978-91-7623-280-4 (pdf)
Recipient's notes	Number of pages 108 / Price
	Security classification

Distributor

Líney Halla Kristinsdóttir, Division of Mathematical Physics, Department of Physics, Sölvegatan 14A, SE-223 62 Lund, Sweden

INTERACTION EFFECTS IN THE TRANSPORT OF PARTICLES IN NANOWIRE QUANTUM DOTS

Líney Halla Kristinsdóttir

LUND
UNIVERSITY

Division of Mathematical Physics
Faculty of Engineering
Lund University

2015

Front cover: An artistic view of the gradual localization of two particles in a nanowire quantum dot, as their interaction strength is increased.

978-91-7623-279-8 (print)
978-91-7623-280-4 (pdf)
Lund-MPh-15/02

Printed in Sweden by Media-Tryck, Lund 2015

CONTENTS

POPULAR SCIENCE SUMMARY

Imagine a wire so thin that its diameter is about one-thousand times thinner than a human hair. That is a nanowire. Now cut the nanowire such that its length is about 1-10 times as long as its diameter. There, we have just pictured a *nanowire quantum dot*[1], roughly like those discussed in this thesis.

The next step is to load some particles, like electrons or atoms, into the nanowire quantum dot. The first intuition might be to picture the particles like balls lying (or bouncing around) in a closed tube. However, in quantum systems, that would not be a correct description. In fact, knowing the precise position of a particle is near as impossible. All you know (if you are lucky) is the probability of the particle's position: You can picture it as a cloud. What is more, in most cases the clouds of all the particles will overlap, making a single cloud.

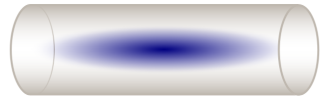

A central topic of this thesis is how the interaction of particles in nanowire quantum dots affects the overall behaviour of the particles. All objects interact with each other, due to gravitation, electromagnetism, collisions, and so on. Examples are the pull we feel towards Earth, a magnet stuck to a fridge, or colliding billiard balls. We will consider two types of interaction:

(i) The Coulomb interaction between electrons in semiconductors;

(ii) The dipole-dipole interaction between dipolar atoms/molecules trapped in vacuum by laser light.

The dipoles can be pictured like rod-shaped magnets: If we bring the north end of one magnet to the south end of another, they will attract (snap together). In turn, if we rotate the magnets so that they are side-by-side with both north

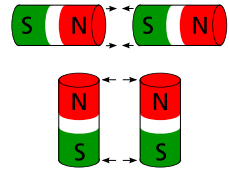

1 A quantum dot, in general, is some kind of a container (typically nanosized) in which the movement of particles, such as electrons or atoms, is hindered in all directions. A distinct feature of quantum dots is that the allowed energy levels are discrete – quantized – like the allowed energy levels of the electron in an atom, which is why quantum dots are often called "artificial atoms".

ends up, they will repel (hard to push together). On the other hand, two electrons will always repel each other.

An interaction effect that is discussed in all the papers that the thesis is based on, is the so called *Wigner localization*[2]. What it boils down to is that when the interaction of particles is strongly repulsive and depends on their relative distance, the particles will position themselves such that the energy of the system is minimized. That is, the particles will localize. At first sight, this may not seem so impressive. However, in quantum systems, localized particles are not at all common: Remember, usually the clouds of all the particles overlap. But when the particles repel each other strongly enough, depending on their relative position, their clouds will separate. One separate cloud for one particle. When you are used to not being able to pinpoint a particle's position at all, that is truly remarkable.

Why would anyone want to investigate interaction effects, such as Wigner localization in nanowire quantum dots? Well, humankind has always had a need to know, understand and explore; be it plants, countries, cultures, people, matter, fate, the weather, and so forth. Sometimes our search for knowledge and understanding has a practical purpose. Sometimes it does not. In science the latter is called fundamental research, to which this thesis belongs. On the other hand I could argue, for example, that since the size of electronic gadgets keeps decreasing, the knowledge of nanosized systems is essential. It really is. But that is not exactly why we do fundamental research on the nanoscale. We are simply curious. Curious as to what laws govern nature and what consequences they have. This thesis is a teeny tiny piece of the immense puzzle making up our knowledge. Perhaps someday, someone will find practical use for it. Perhaps.

2 Named after Eugene Wigner who predicted it in 1934 for bulk material (the opposite of quantum dots, that is free movement in all directions), in which case the phenomenon is called Wigner crystallization.

ALMENN SAMANTEKT

Ímyndaðu þér vír sem er svo grannur að þvermál hans er einungis um einn þúsundasti af mannshári. Þetta er nanóvír. Klipptu nú vírinn þannig að lengd hans verði um 1-10 sinnum meiri en þvermálið. Sko til, við höfum nú nanóvírsskammtapunkt[3] í höndunum, um það bil eins og þá sem þessi ritgerð fjallar um.

Næsta skref er að koma einhverjum eindum, t.d. rafeindum eða frumeindum, fyrir í nanóvírsskammtapunktinum. Í fyrstu sér maður eindirnar kannski fyrir sér sem litlar kúlur í lokuðum hólki. Í skammtakerfum er slík mynd aftur á móti ekki alls kostar rétt. Raunar er það hér um bil ómögulegt að vita nákvæma staðsetningu eindar. Það eina sem við þekkjum (ef við erum heppin) eru líkurnar á staðsetningu hennar: Þú getur ímyndað þér eindina eins og ský. Að auki skarast oftast ský allra eindanna, svo úr verður eitt ský.

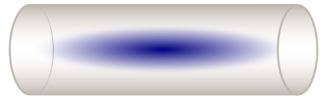

Eitt helsta viðfangsefni þessarar ritgerðar er hvernig víxlverkun einda í nanóvírsskammtapunkti breytir almennri hegðun þeirra. Allir hlutir víxlverka við hvern annan vegna þyngdarafls, rafsegulmagns, árekstra og svo framvegis. Dæmi um víxlverkanir eru togkrafturinn sem við finnum gagnvart Jörðinni, segull fastur á ísskáp eða árekstrar lottókúlna. Við munum skoða tvenns konar víxlverkun:

(i) Coulomb-víxlverkun rafeinda í hálfleiðurum;

(ii) Tvípólsvíxlverkun milli frum- eða sameinda sem eru lokaðar af í lofttæmi með leisigeislum.

Það má sjá tvípól fyrir sér líkt og stangarlaga segul: Ef við færum norðurenda eins seguls að suðurenda annars seguls, þá dragast þeir að hvor öðrum (smella saman). Ef við snúum tveim seglum þannig að þeir séu hlið við hlið, báðir með

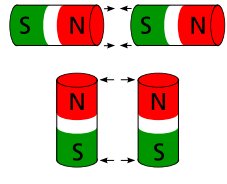

3 Skammtapunktur er almennt einhvers konar ílát (gjarna í nanóstærð) þar sem hreyfing einda eins og rafeinda og frumeinda, er takmörkuð í allar áttir. Eitt helsta sérkenni skammtapunkta er að leyfileg orka eindanna er strjál – skömmtuð – eins og leyfileg orkuástönd rafeinda í frumeind. Af þessari ástæðu eru skammtapunktar gjarna kallaðir „gervifrumeindir“.

norðurendann í sömu átt, þá hrinda þeir hvor öðrum frá sér (erfitt að þrýsta þeim saman). Tvær rafeindir munu aftur á móti alltaf hrinda hvor annarri frá sér.

Víxlverkunarhrif sem fjallað er um í öllum greinunum sem ritgerðin byggir á eru hin svokallaða *Wigner-staðbinding*[4]. Í grunninn snýst hún um að þegar víxlverkun einda er mjög fráhrindandi og er háð fjarlægðinni milli eindanna, þá munu eindirnar staðsetja sig á þann hátt að orkan í kerfinu er í lágmarki. Með öðrum orðum, þá verða eindirnar staðbundnar. Í fyrstu virðist það kannski ekki svo merkilegt. En staðbundnar eindir eru alls ekki venjan í skammtakerfum: Mundu, oftast renna ský allra eindanna saman í eitt ský. En þegar eindirnar hrinda hver annarri nógu sterkt frá sér, háð fjarlægð, þá greinast skýin að. Eitt ský fyrir hverja eind. Þegar maður er vanur því að geta alls ekki ákvarðað staðsetningu eindanna, þá er það svo sannarlega magnað.

En hvers vegna skyldi nokkur hafa áhuga á að rannsaka víxlverkunarhrif, eins og Wigner-staðbindingu í nanóvírsskammtapunktum? Jú, mannkynið hefur alltaf fundið þörf fyrir að vita, skilja og skoða, hvort sem um ræðir plöntur, ókunnug lönd, menningu, fólk, efni, örlög, veðrið o.s.frv. Stundum leiðir þessi þekkingarleit okkar til augljósrar hagnýtingar. Stundum ekki. Í vísindum er hið síðarnefnda kallað grunnrannsóknir og þessi ritgerð tilheyrir þeim. Ég gæti að vísu fullyrt að þar sem stærð raftækja minnkar stöðugt, þá sé þekking á nanókerfum bráðnauðsynleg, svona til dæmis. Það er alveg satt. En það er samt ekki hin raunverulega ástæða fyrir grunnrannsóknum á nanókvarða. Við erum einfaldlega forvitin. Við viljum vita hvaða lögmál ríkja í náttúrunni og hverjar afleiðingar þeirra eru. Þessi ritgerð er agnarsmá viðbót við þekkingu okkar. Kannski mun finnast hagnýting á henni einhvern daginn. Kannski.

4 Fyrirbærið er nefnt eftir Eugene Wigner sem spáði fyrir um það árið 1934 fyrir almennt efni þar sem hreyfing rafeindanna er frjáls í allar áttir (andstæða skammtapunkta). Í því tilviki er talað um Wigner-kristöllun.

ACKNOWLEDGEMENTS

I owe my deepest gratitude to Steffi, my supervisor. Thank you for believing in me, for guiding me in the right direction, while still allowing me to choose freely. Thank you for your insight. You have taught me many great lessons, and for sure not all of them are about physics. And Andreas, my inofficial co-supervisor. Thank you for your guidance and insightful perspective, for bringing me from the abstract world of theoretical simulations to experimental data. Thank you both, Steffi and Andreas, for your uncanny ability to point out the assets among my mishmash of results, every time that I lose sight of the forest for the trees.

A big thank you to my former and current fellow group members: Jonas, Sara, Jeremy, Frank, Georg, Peter, Georgios, Andrea, Francesc, Gunnar, Elife, Johannes, Yousef, Jakob. You are like a big dear family. Also my other collaborators at Matfys, Olov and Susanna. Thank you!

Sofia and Heiner, Henrik, Hongqi and Lars, my collaborators at Solid state physics. Thank you for all the great ideas and inspiring discussions.

Sven, our wonderful head of divison, and everybody else at Matfys, in the past and present. Thank you for making Matfys a great workplace. I'll miss you all and the lunch discussions, Friday fika, and the annual goose dinner.

Katarina and Cecilia, you certainly deserve a special mention. You truly are life savers, each in your own way.

Gillis and Bahareh, my perfect office mates. Thank you for an easy, quiet and friendly atmosphere. Bahareh: you and Yousef are too kind for your own good, thank you for everything! Also Hailiang and Gita – it was a short but nice time.

Valeria, my chocolate collaborator. Thanks for reminding me to eat my chocolate and enjoying it with me. (Seriously, it gets too old without you here at Matfys.)

Students of the Linnaeus graduate school and at the nmC@LU. Thanks for all the fun and your great company during workshops, courses, and retreats. Especially those of you who organized various events, seminars, and other fun things to do.

The Icelandic Choir in Lund. My stay in Lund would definitely not have been as fun and satisfying without you. Thanks for the crisis counsels during the economic meltdown, for the singing in and out of tune, the "jú-jú-jú" and hip-flexing (Hulda Birna), for all the 1. des. balls (Sverrir), the 1. maí concerts and barbeques (Haukur), the choir camps, the extra rehearsals at home (Draumey, Nonni), and for being there and simply making life so fun.

Our many Icelandic neighbours, the big family at Kjamminn. Especially the Housewife Mafia for the Sunday-saumó, getting me to start playing badminton again, and all the discussions of your first hand experience with all kinds of problems that you encounter with small children. Despite being childless at the time, I sure was never bored.

My current badminton buddies: Addý, Ingibjörg and Berglind. You make me run and sweat and laugh and truly have fun. You girls rock!

Saumaklúbburinn Sæmundur: Guðrún, Silla, Þórhildur, Silja Björk, Hanna, Anna Sigga, Elín, María Svavars, Anna (amma)... you really are the best. Thanks for all the cakes, chat, gossip, laughs, knitting (and undoing), crocheting (and undoing), spontaneous lunch meetings, and just being a great bunch of friends.

Viðar. Thanks for pointing out to me back in 2008 that I might find the research done in Stephanie Reimann's group interesting; it might be a good place for me to do a master's project. It sure was. And since I've started: Thanks for being a great teacher and mentor, always having a minute or two for a discussion.

The family at Staður, Reykjanes. It was the best decision of my life to go and be your kúarektor. The memory of my summers with you (way too) many years ago is always an encouragement. They really were wonderful and a great lesson for life. So

thank you all, Fríða & Eiríkur, Gauti, Rebekka & Stjáni, Harpa, and, yes, Unnur, I know you're out there somewhere keeping an eye on things!

Ásta, Hulda Soffía, Kristín Þóra, Kristjana, Unnur. Thanks for always being there and all the great times we have had together in the past and sure will have in the future!

My wonderful big family in Iceland, Sweden, Denmark, Germany... Always there with a helping hand. Ready with a bed for guests, a table laden with good food, and a relaxed conversation. I'm so grateful for having all of you.

Guðný, Jóndór, Harpa & Maggi, and Sylvía, my wonderful, loving and caring in-laws. Getting to know you in the past 9 years felt like winning the lottery, over and over again. Thank you for all the support, your kindness, and simply for who you are.

Amma og afi í Sigtúni, amma og afi á Akureyri. Þið gáfuð mér svo margt. Skyr með miklum sykri og rjóma, lúbarinn harðfisk á steini út í garði, fjöruferðir og bílabrjóstsykur, kleinur og soðbrauð, rommí og vist og lander og manna, sund á hverjum degi. En það verðmætasta af öllu var samveran, tíminn með ykkur. Þúsund þakkir!

Baldur, Birte, Matthías and Bjarki; Bjarnheiður & Bergur. Thanks for being the best siblings, sister/brother-in-law and nephews I could have wished for. I look so much forward to seeing you more often than in the past years.

Pabbi & mamma. I believe I can never thank you enough. For believing in me, for supporting me in everything I do. For all the help, whatever small or big obstacle is at hand (even in situations that make you hop on a plane with less than 36 hours' advance). Thank you.

Finally, my sincere gratitude to the love of my life Sigurður Ægir, for your constant support, delicious cooking, patience and love. And our dear son Jón Sölvi, for never failing to make me forget all about work and everyday chores. You two give life its depth and bright colour.

LIST OF PUBLICATIONS

The thesis is based on the following publications:

I L. H. Kristinsdóttir, J. C. Cremon, H. A. Nilsson, H. Q. Xu, L. Samuelson, H. Linke, A. Wacker, S. M. Reimann. *Signatures of Wigner localization in epitaxially grown nanowires.* Physical Review B **83**, 041101(R) (2011). (Editor's choice.)

II L. H. Kristinsdóttir, O. Karlström, J. Bjerlin, J. C. Cremon, P. Schlagheck, A. Wacker, S. M. Reimann. *Total current blockade in an ultracold dipolar quantum wire.* Physical Review Letters **110**, 085303 (2013).

III L. H. Kristinsdóttir, J. Bengtsson, H. Linke, S. M. Reimann, A. Wacker. *Thermopower as a tool to investigate many-body effects in quantum systems.* Applied Physics Letters **105**, 083105 (2014).

As PhD student I have also co-authored the following publications, that are not included in the thesis:

- L. H. Kristinsdóttir, Ó. G. Flóvenz, K. Árnason, D. Bruhn, H. Milsch, E. Spangenberg, J. Kulenkampff. *Electrical conductivity and P-wave velocity in rock samples from high-temperature Icelandic geothermal fields.* Geothermics **39**, 94-105 (2010).
- H. Milsch, L. H. Kristinsdóttir, E. Spangenberg, D. Bruhn, Ó. G. Flóvenz. *Effect of the water-steam phase transition on the electrical conductivity of porous rocks.* Geothermics **39**, 106-114 (2010).
- M. S. Jaya, S. A. Shapiro, L. H. Kristinsdóttir, D. Bruhn, H. Milsch, E. Spangenberg. *Temperature dependence of seismic properties in geothermal rocks at reservoir conditions.* Geothermics **39**, 115-123 (2010).

To my family

Ef þú smælar framan í heiminn, þá smælar heimurinn framan í þig.

Megas

(His characteristic version of 'If you smile to the world, the world will smile back at you')

PROLOGUE

It's all about the journey, not the destination.

As stated by many wise people

1

INTRODUCTION

All objects interact with each other via some kind of a force; gravitational, electromagnetic, collisional, etc. Sometimes the interaction is so small relative to other influencing factors that it can be neglected. In most cases, however, the interaction cannot be overlooked. Down on the nanoscale, the interaction between particles can provide interesting quantum physical phenomena, for example Wigner crystallization, current blockade, pairing, or the fractional quantum Hall effect, to name only a few. Different types of interaction – short- or long-range, repulsive or attractive, isotropic or anisotropic – may result in different effects. These can appear, for example, in the energy spectrum of the system.

The work presented in this thesis aims at the theoretical description of semiconductor quantum dots (Paper I and Paper III), for which the energy spectrum can be experimentally obtained by transport spectroscopy. We will also look at a system of an ultracold atom gas with transport spectroscopy in mind (Paper II). This is unusual, as the particle density or the momentum distribution are the prevailing

measurable quantities. However, the experimental breakthrough by Brantut *et al.* [12] has made transport spectroscopy with ultracold atoms a feasible option. This encouraged an adjustment of our semiconductor nanowire model to describe atom traps as well. The controllability and cleanness of such systems offers a great opportunity to explore a host of quantum physical phenomena, that are inaccessible in semiconductors due to unavoidable perturbations of various kinds, for example.

This thesis presents a theoretical study, focusing on the effects of interaction in nanosystems. Many of the most readily available theoretical methods only provide the ground state, or they are only valid for weak interactions. However, as explained further below, in order to study the quantum transport and an interaction effect called Wigner localization we also need information on e.g. the excited states. If one is content with systems of very few particles (for example, up to 10 at maximum in case of strong interaction) the full energy spectrum is accessible by exact diagonalization, also known as the configuration interaction method (see e.g. refs. [16, 65] for an overview). Furthermore, this method, in fact, provides the exact eigenstates of the system. From those we can derive, for example, the particle density and information on how the system couples to leads/reservoirs. That way we can model the transport of particles through the system, both in order to compare our results with experiments, but also to look for interesting consequences of the particles' interaction in the quantum-mechanical properties of the system.

In the following we briefly introduce some of the main aspects of this thesis: The general model system, Wigner localization, the specific interactions and systems considered, and the concept of thermopower. In chapter 2 we will take a brief look at the numerical methods used in the calculations. In chapter 3 the main results of the papers, and my contribution to them, will be summarized. In chapter 4 some preliminary results are discussed. An outlook is given in chapter 5. Finally, the papers are reprinted at the end of the thesis.

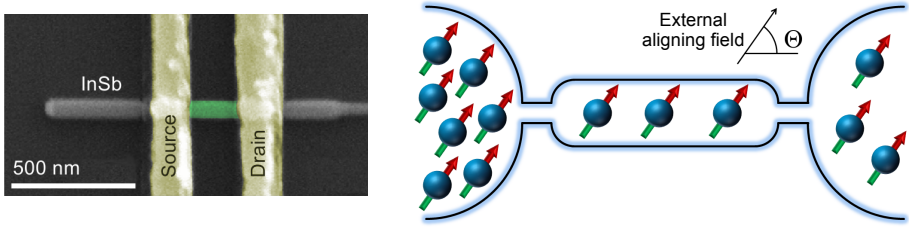

(a) InSb nanowire. **(b)** Ultracold dipolar gas.

Figure 1.1 The two systems under study. **(a)** Scanning electron microscope (SEM) image of an InSb nanowire. Gold strips (source/drain, yellow shaded) are grown on top, defining a quantum dot (green shaded) with Schottky barriers at the interface. (Modified from Paper I.) **(b)** Schematic illustration of an ultracold gas of dipolar atoms/molecules. A narrow channel of dipolar particles is connected to two reservoirs (left/right). The dipole moments of the particles are aligned at an angle Θ by an external field. (Modified from Paper II.)

1.1 A VERSATILE MODEL FOR THE GENERAL SYSTEM

The systems that we study are at first sight quite disparate: A semiconductor nanowire (figure 1.1(a)) and a gas of ultracold atoms in a magneto-optical trap (as schematically shown in figure 1.1(b)). Nevertheless, the same physical model can be used to describe them. A schematic picture of the general system is shown in figure 1.2, along with the potential across the system. A nanowire quantum dot[1] is connected to two leads (particle reservoirs) with a potential barrier in between. There are many features in the model that can be changed: The type of confinement in the transversal directions, the length and width of the quantum dot, the height and width of the barriers, the type and strength of interaction in the quantum dot, the effective mass of the particles in the dot, barriers and leads, and the spin of the particles. Furthermore, the key ingredients in transport spectroscopy can be varied as if we were in the laboratory: We can change the temperature of either lead, apply a potential bias V_{sd} between source and drain, and change the gate potential μ_{gate}. On the other hand, there are properties that are fixed: The

1 In this thesis, a *nanowire quantum dot* should be understood as a system that is confined in all three spatial dimensions, where the confinement in the transversal directions is (much) tighter than in the longitudinal direction.

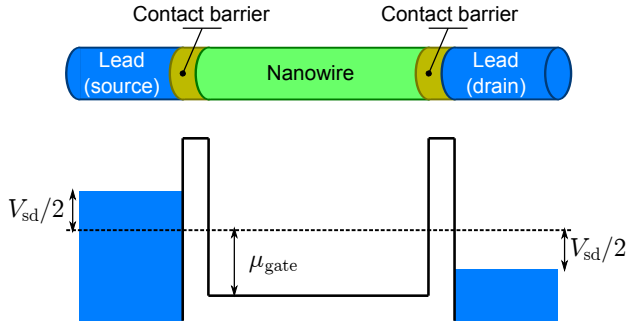

Figure 1.2 A schematic of the general model system; a quasi-one-dimensional nanowire coupled to two leads (particle reservoirs). The potential across the system and some of the parameters used to control it are shown in the lower panel. See further discussion in text.

statistics of the particles (here we deal only with fermions), the description of the leads by a Fermi sea, and a maximum of 8-10 particles in the quantum dot. Here, we also restrict ourselves to one particle tunneling at a time (1st order transport), and assume a flat bottom potential (finite well) along the nanowire. This last restriction, however, can be remedied, as the use of B-splines allows us to use, in principle, an arbitrary potential in the longitudinal direction, as further discussed in section 2.1.3.

1.2 WIGNER LOCALIZATION

A recurring topic in all three papers is a phenomenon called Wigner localization. This is a certain state of matter due to interaction, that was first predicted for bulk material by Wigner in 1934 [80] and is in that case well known as Wigner crystallization. It is a fairly intuitive notion. Assume that the interaction between particles is long-range and repulsive and only depends on their relative distance, not on their actual position. If the interaction is so strong that it is the dominating factor in the system, then the particles will seek to position themselves such that

the system energy is minimized: They will crystallize. As it is rather superfluous to talk of a crystal in a few-body system, the term *Wigner localization* was coined. (See the review by Reimann and Manninen [65].)

Let us take a closer look at a two-body system, as the simplest possible case for interacting spin-half fermions. We consider two limiting cases. Firstly, if the particles are noninteracting, see figure 1.3(a), the system is described by the independent particle shell-model: The many-body states are simply formed by filling a number of single-particle levels and applying the proper statistics (and hence, the Pauli exclusion principle). As can be seen from figure 1.3(a), the 1-body and 2-body excitation energies coincide in this case, $\Delta\epsilon = \Delta E_2$.

Secondly, when strong repulsive interactions dominate the system, Wigner localization may occur. The two fermions are then spatially separated, see figure 1.3(b). In this case, the Pauli exclusion principle has no effect. Hence, there is practically no difference between the singlet groundstate and the triplet 1st excited state. As a consequence, the excitation energy of the two-body state becomes negligible, $\Delta E_2/\Delta\epsilon \ll 1$.

It is our aim to find a signature of Wigner localization that can be used for comparison with experimental data. As stated before, the excitation spectrum of the system is accessible by transport spectroscopy. However, it only provides the excitation energies (energy difference between the groundstate and the excited states), while it does not distinguish between states of the same energy. Hence one cannot determine right away if the singlet ground state and triplet 1st excited state have merged into one 4-fold degenerate state. One way would be to apply a homogeneous magnetic field to the system and thereby see the triplet state split up. If one can tune the interaction strength, another possibility is to see the singlet and triplet states separate as one decreases the interaction strength. Furthermore, we can define an intermediate stage, the *onset of Wigner localization*[2], where the singlet ground state and triplet 1st excited state are very close but have not yet merged,

2 This regime is also known as *incipient Wigner localization*, see for example refs. [66, 37, 38].

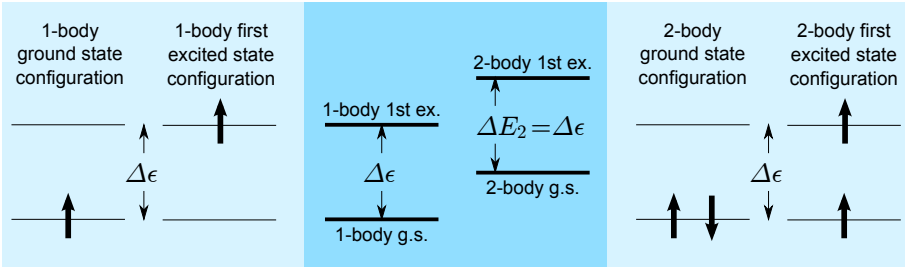

(a) Zero interaction.

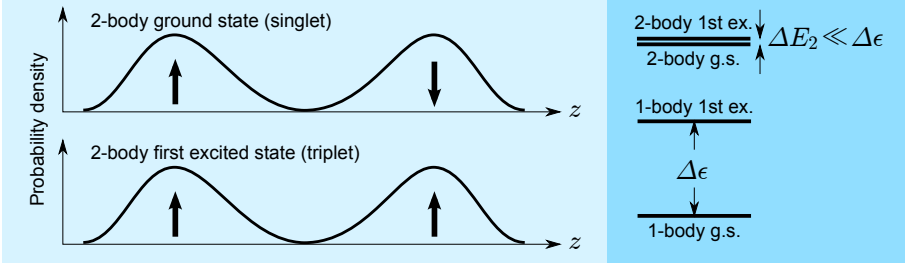

(b) Wigner localization.

Figure 1.3 Two extremes in interaction strength of spin-half fermions. **(a)** Noninteracting particles. The system is simply described by the independent particle shell-model: N-body states are obtained by ordering N particles into single-particle levels, taking the Pauli exclusion principle into account, see the left and right panel for $N = 1$ and $N = 2$, respectively. Hence, the excitation energies of one particle ($\Delta\epsilon$) and two particles (ΔE_2) are equal, see the centre panel. **(b)** Wigner localized particles (strong repulsive interaction). Left panel: Since the particles are localized, i.e. their densities have negligible overlap, the Pauli exclusion principle has negligible effect. Therefore, there is hardly any difference between the singlet groundstate and triplet 1st excited state. Right panel: Consequently, the 2-body excitation energy is negligible compared to the 1-body excitation energy, $\Delta E_2/\Delta\epsilon \ll 1$. See further discussion in text.

characterized by the condition that ΔE_2 is significantly smaller than $\Delta\epsilon$, in short $\Delta E_2 < \Delta\epsilon$. Of the previously enumerated signatures of Wigner localization, the last one is the easiest to determine in an experiment.

1.3 ELECTRONS IN SEMICONDUCTORS

We need a long-range interaction to obtain Wigner localization [78]. One of the best known long-range interactions is *Coulomb interaction*, the interaction between two charges. This is, for example, the interaction found between conductance electrons in semiconductor nanowires, and the one considered by Wigner in his original paper [80]. The Coulomb interaction between two point particles of charge q_1 and q_2 is given by [46]

$$v_C(r) = \frac{q_1 q_2}{4\pi\varepsilon}\frac{1}{r} \tag{1.1}$$

where $r = |\mathbf{r}_1 - \mathbf{r}_2|$ is the distance between the particles and ε is the dielectric permittivity of the surrounding material. For electrons, the strength of the interaction is $u_C = e^2/(4\pi\varepsilon a)$, where e is the elementary charge, and a is the length scale of the problem (here, the half-length of the nanowire). However, it has to be considered in relation to other energy scales of the system, i.e. that of the kinetic energy ($\sim \hbar^2/ma^2$). This leads to the effective interaction strength

$$\tilde{u}_C = \frac{e^2}{4\pi\hbar^2}\frac{ma}{\varepsilon} \tag{1.2}$$

where m is the effective mass of the electrons. Once the material for the nanowire has been chosen (ε, m), the only parameter left to tune the effective interaction strength is the length of the nanowire[3], $2a$.

3 The different dielectric constants of the nanowire and the surrounding material affect the interaction of the electrons in the nanowire, as will be discussed in appendix A. Choosing a material with high dielectric constant for the nanowire may enhance localization of the electrons [56]. However, the dielectric constants of a nanowire quantum dot device cannot be changed post-fabrication.

The feasibility of tuning the length of a semiconductor nanowire in an experiment was considered. In most realistic cases, however, it is either highly impractical or impossible. The use of finger gates, where many gate electrodes are grown side by side across the nanowire [32], was examined. It was, however, rejected due to the complexity of such nanodevices, and since the presence of a finger gate, albeit inactive, may affect the potential across the nanowire. It is, furthermore, not a feasible option to change the spacing of the leads. In some cases the spacing is already fixed during the growth of the nanowire, such as in heterostructure InAs-InP nanowires. It is in any case impractical to grow or remove contacts from a complete nanowire device.

We can, therefore, rule out the possibility of externally tuning a semiconductor nanowire system from an effectively noninteracting state to a Wigner localized state. Apart from that drawback, there is always the problem of defects (impurities, bending, etc.) in semiconductor nanowires. A long nanowire is needed for Wigner localization ($\tilde{u}_C \propto a$), while it is extremely hard, if not impossible, to produce a clean nanowire that is long enough, as we experienced while preparing Paper I. Therefore, we seek an alternative system with a different long-range interaction.

1.4 ULTRACOLD DIPOLAR GASES

Systems of ultracold atoms and molecules present an enormous potential of clean and highly tunable mesoscopic systems [9]. The experimental techniques to work with optical traps containing just a few particles already exist [71]. Furthermore, the prospect of transport spectroscopy is very promising [12] and controlled thermotransport has recently been realized [11].

The most common interaction in ultracold systems is the contact interaction [39]. However, as the name implies, it is a zero-range interaction, and is therefore unsuitable for studying Wigner localization. Another interaction that has gained more attention recently is the long-range *dipole-dipole interaction* [4, 52], e.g. due to its

potential use in quantum computing [69]. This is the interaction between particles that have an electric or magnetic dipole moment. Examples of particles with a magnetic dipole moment are chromium, erbium and dysprosium atoms [51, 55, 1]. On the other hand, Rydberg atoms [54, 36] and some diatomic molecules, for example, exhibit an electric dipole moment[4].

When the dipole moments of dipolar particles are aligned by an external field, the dipole-dipole interaction is given by [46, 73]

$$v_{\mathrm{dd}}(r) = \frac{d^2}{r^3}\left(1 - 3\cos^2(\theta_{\mathrm{rd}})\right) + \frac{4\pi}{3} C d^2 \delta^3(\mathbf{r}) \tag{1.3}$$

where θ_{rd} is the angle between the particle separation $\mathbf{r}$ and the electric dipole moment $\mathbf{p}$ (or the magnetic dipole moment $\boldsymbol{\mu}$), d^2 is the coupling strength, and $C = 1$ for electric dipoles ($C = -2$ for magnetic dipoles). In case of electric dipoles, $d^2 = p^2/(4\pi\varepsilon_0)$ where ε_0 is the vacuum permittivity. For magnetic dipoles, the dipole coupling ($d^2 = \mu_0\mu^2/(4\pi)$ where μ_0 is the vacuum permeability) is significantly weaker than for electric dipoles [52].

Note from eq. (1.3) that the long-range interaction is anisotropic: It ranges from repulsive to attractive, depending on the relative position and orientation of the dipoles, see figure 1.4. For strong dipolar interactions, it is therefore necessary to confine the dipolar gas in one or two dimensions in order to stabilize the dipolar gas against collapse [49, 59].

The effective strength of the long-range term of the dipole-dipole interaction (when scaled relative to the kinetic energy, $\sim \hbar^2/ma^2$) is

$$\tilde{u}_{\mathrm{dd}} = \frac{md^2}{a\hbar^2}\left(1 - 3\cos^2\theta_{\mathrm{rd}}\right) . \tag{1.4}$$

4 Rydberg atoms are excited atoms, e.g. rubidium or caesium, where one or more of the electrons are excited to orbitals with very high principal quantum number. Examples of polar molecules, that have been trapped and cooled successfully in the rovibrational ground state, are KRb [58, 63] and LiCs [23].

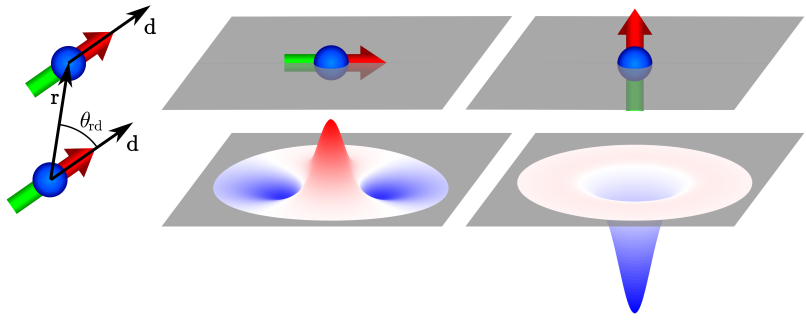

Figure 1.4 The anisotropic dipole-dipole interaction depends on θ_{rd} (the angle between the dipole moment $\mathbf{d}$ and the vector $\mathbf{r}$ connecting the dipolar particles) and falls off with $1/r^3$. The interaction potential felt by a dipolar particle in the two dimensional plane, whose dipole moment is aligned with the dipole moment of the reference particle above the plane (blue ball), is depicted in two cases: The interaction is mainly repulsive (red, positive) when the dipoles are side-by-side (parallel to the plane), whereas it is attractive (blue, negative) when the dipoles are aligned head to tail (perpendicular to the plane).

This tells us, firstly, that shortening the quantum dot effectively increases the relevance of the interaction. Secondly, and more importantly, we can tune the interaction externally by changing the direction of the electric (or magnetic) field that aligns the dipole moments of the particles. In one dimension, the sign of the interaction is homogeneous, such that the particles' interaction can be tuned, externally, from strong repulsion to noninteracting and even further, into the attractive regime (see figure 2.1). The tunability of the interaction is explored, for example, in ref. [21] and Paper II.

1.5 THE SEEBECK EFFECT

In 1821, Thomas Johann Seebeck discovered that a temperature difference across metals causes charge carriers to diffuse, creating an electric current[5]. This is the well known Seebeck effect (which, together with the Peltier effect and Thomson effect, comprises the thermoelectric effect). The utilization of the Seebeck effect, turning waste heat into electricity, is highly desirable, both from an economical and environmental perspective. It has, however, proved extremely difficult, as a prospective thermoelectric material relies on three parameters: electrical conductivity, thermal conductivity, and thermopower (the Seebeck coefficient). These parameters are interdependent in a way that makes the thermoelectric efficiency of usual materials too low. On the other hand, turning to nanoengineered materials has provided a substantial increase in the largest achieved thermoelectric efficiency (or, more precisely, the thermoelectric figure of merit) during the past two decades [45].

However, our interest in the Seebeck effect in nanostructures also lies in its use as a characterization tool. The voltage bias that the temperature difference ΔT creates, the thermovoltage, is given by

$$V_{\mathrm{th}} = -S\Delta T \tag{1.5}$$

where S is the *Seebeck coefficient* or *thermopower*. It has been shown that excited states in quantum dots appear as fine structure (dips) in the thermopower at low enough temperatures [7, 27, 26]. Therefore, the excitation energies, such as $\Delta\epsilon$ and ΔE_2, may be determined from the thermopower (see figure 2.7). Thermopower can thus be used to detect the onset of Wigner localization, as discussed in Paper III.

5 In fact, Seebeck thought the temperature difference induced a magnetic polarization [70], not an electric current. He conducted his experiments on a ring of copper, joined into a closed loop by a second metal (antimony, bismuth, etc.). By heating one junction (at first, unintentionally by his hand), Seebeck observed the deviation of a suspended magnetic needle, and therefore interpreted his discovery as a magnetic effect. It was Hans Christian Ørsted who correctly attributed the deviation of the magnetic needle to an electric current in the metallic loop (that induces a magnetic field by Ampère's law) and coined the term *thermoelectricity* [13].

2

METHODS

As outlined in the Introduction, the problem at hand is to simulate transport of fermions in a nanosystem consisting of a quantum dot and two leads, with significant interaction of particles in the quantum dot. The main goal is to explore the effects of the interaction, such as Wigner localization.

For transport through noninteracting systems or systems with weak interaction (such that the system can be described as effectively noninteracting), the Landauer-Büttiker formalism provides a good description [22]. Transport through interacting systems in general is, however, a different matter. Various methods of varying complexity exist. To our purposes, the Bardeen transfer Hamiltonian method [5, 25] becomes a natural choice, as it allows for a full many-body treatment of the quantum dot. In this approach the system is described by the Hamiltonian

$$\hat{H} = \hat{H}_{\text{dot}} + \hat{H}_{\text{leads}} + \hat{H}_{\text{tunneling}} \tag{2.1}$$

where $\hat{H}_{\text{dot}}$, $\hat{H}_{\text{leads}}$ and $\hat{H}_{\text{tunneling}}$ describe the dot, leads, and tunneling between states in the dot and leads, respectively. This entails that we treat the barriers between the quantum dot and the two leads as a perturbation, assuming that the transmission through the barriers is very small. In other words, instead of trying to work on the whole system at once, we treat the systems of the quantum dot and the leads separately, and subsequently handle the transport of particles between the dot and the leads.

The chapter is organized as follows: The exact many-body approach to the quantum dot is presented in section 2.1, while the treatment of the leads is briefly described in section 2.2, and the transport formalism is detailed in section 2.3. The basics of charge stability diagrams, by which results of transport simulations and experiments are frequently presented, are given in section 2.4. Finally, thermopower and its use for detecting the onset of Wigner localization is briefly described in section 2.5.

2.1 FINDING THE "EXACT" STATES OF A NANOWIRE QUANTUM DOT

The quantum dot Hamiltonian, $\hat{H}_{\text{dot}}$, is in general given by

$$\hat{H}_{\text{dot}} = \hat{H}_0 + \hat{V}_{\text{int}} \tag{2.2}$$

where $\hat{H}_0$ is a one-body operator, including e.g. the kinetic energy and the confining potential, and $\hat{V}_{\text{int}}$ is the two-body interaction between the particles. We want to investigate how the interaction affects the system, that is, find the energy spectrum and the probability density of the states. The most difficult part of that task is, in general, how to handle the interaction, $\hat{V}_{\text{int}}$.

There exists a number of different ways to model the system and the available methods to obtain the necessary information about the system can be implemented in

various ways. There are mean field methods, such as the Hartree-Fock method or the Gross-Pitaevskii method, that effectively turn the two-body interaction into a one-body problem. These methods work very well for weak interactions, but typically fail for increased correlations. There are more advanced methods, such as density functional theory, quantum Monte Carlo, Green's functions, and exact diagonalization. All of these methods are exact in principle, but require some approximations in practice, due to lack of e.g. computational power or information. The different methods provide a varying amount of information on the system: Quantum Monte Carlo methods typically only provide the ground state, while exact diagonalization can give excited states as well; and Green's functions give any observable one needs, while exact diagonalization provides the full wave function.

Our method of choice is *exact diagonalization* (see, e.g., refs. [16, 68, 67, 65]), also known as *configuration interaction method* in quantum chemistry [19]. This method allows one, in principle, to calculate the states and whole energy spectrum of the system up to an arbitrary accuracy. However, the computational power needed increases exceedingly fast with the particle number and the degrees of freedom of the system. Furthermore, strong interaction is more demanding, especially if it is attractive. In practice, this restricts the applicability of the method to systems of, for example, up to $\sim$10 particles, one to two dimensions, and strong repulsive/weak attractive interaction. However, when working within the boundaries set by the computers of today, it is an extremely powerful method.

The numerical implementation of the exact diagonalization method used in this thesis is incorporated in a library called `cimethod`. A description of the `cimethod` library along with a number of applications can be found in ref. [20].

2.1.1 EXACT DIAGONALIZATION METHOD

The aim of the exact diagonalization method is to find the states $|a\rangle$ and energy levels E_a of $\hat{H}_{\text{dot}}$, that is, solve the eigenvalue problem $\hat{H}_{\text{dot}}|a\rangle = E_a|a\rangle$ (i.e. the time-independent Schrödinger equation). The main idea is to expand the eigen-

states $|a\rangle$ in a complete many-body basis, and thus turn the eigenvalue problem into the diagonalization of a matrix.

The exact diagonalization method is formulated within second quantization (see refs. [41, 34], for example). Thus the aforementioned many-body basis consists of Fock states, $|\mathbf{n}\rangle$, based on a suitably chosen complete set of single-particle states, $\{|\phi_i\rangle\}$. The most natural choice of $|\phi_i\rangle$ are the single-particle eigenstates of $\hat{H}_0$ with eigenenergy ϵ_i. Hence, within second quantization, the Hamiltonian becomes

$$\hat{H}_{\mathrm{dot}} = \sum_{i=1}^{\infty} \epsilon_i \hat{d}_i^\dagger \hat{d}_i + \frac{1}{2} \sum_{i,j,k,l=1}^{\infty} V_{ijkl} \hat{d}_i^\dagger \hat{d}_j^\dagger \hat{d}_l \hat{d}_k \tag{2.3}$$

where $\hat{d}_i^\dagger$ ($\hat{d}_i$) is the creation (annihilation) operator of a particle in state $|\phi_i\rangle$, and

$$V_{ijkl} = \iint \phi_i^*(\mathbf{x}) \phi_j^*(\mathbf{x}') v(\mathbf{x}, \mathbf{x}') \phi_k(\mathbf{x}) \phi_l(\mathbf{x}') \, \mathrm{d}\mathbf{x} \, \mathrm{d}\mathbf{x}' \tag{2.4}$$

is the interaction integral[1]. Here $\mathbf{x} \equiv (\mathbf{r}, \sigma)$ is the combined spatial and spin coordinate, $\phi_i(\mathbf{x})$ is the wave function of single-particle state $|\phi_i\rangle$, and $v(\mathbf{x}, \mathbf{x}')$ is the interaction. The matrix formulation of the eigenvalue problem becomes

$$\begin{bmatrix} \langle \mathbf{n}_1 | \hat{H}_{\mathrm{dot}} | \mathbf{n}_1 \rangle & \langle \mathbf{n}_1 | \hat{H}_{\mathrm{dot}} | \mathbf{n}_2 \rangle & \cdots \\ \langle \mathbf{n}_2 | \hat{H}_{\mathrm{dot}} | \mathbf{n}_1 \rangle & \langle \mathbf{n}_2 | \hat{H}_{\mathrm{dot}} | \mathbf{n}_2 \rangle & \cdots \\ \vdots & \vdots & \ddots \end{bmatrix} \mathbf{a} = E_a \mathbf{a} \tag{2.5}$$

where $\mathbf{a} = (a_1, a_2, \ldots)$ is the vector representation of the state $|a\rangle = \sum_{\nu=1}^{\infty} a_\nu |\mathbf{n}_\nu\rangle$.

In practice, there are a few obstacles to overcome. It is evident from eq. (2.5), that the matrix we wish to diagonalize is infinite. This is, of course, impossible and consequently the basis must be cut off. To that end, the most common way is either to include Fock states only up to some cut-off energy, or to restrict the number of single-particle states used to build the Fock states. The low-lying energy

1 The interaction integrals V_{ijkl} will play a central role in the next subsection.

states can thus, in principle, be calculated up to an arbitrary accuracy by including an ever larger number of basis states.

However, the many-body basis size increases extremely fast with increasing number of single-particle basis states and the number of particles in the system, while computational power, such as the working memory, is a limited resource. In order to reach convergence for systems of three or more particles, one usually has to impose some conditions on the system to reduce its dimensionality and/or exploit some symmetries of the Hamiltonian. For example, one may assume that the particles are spin-polarized. Another example, in the case of cylindrically symmetric systems, is the use of conservation of angular momentum: The matrix in eq. (2.5) can thus be made block-diagonal, and thereby the computational problem is split into many smaller pieces. Yet another example to aid convergence is provided in the following subsection.

2.1.2 QUASI 1-DIMENSIONAL SYSTEMS: EFFECTIVE INTERACTION

Assume that the confinement in two of the three spatial dimensions, say x and y, is much stronger than in the third direction, z. Consequently, excitations in x and y are much more expensive than several excitations in z. Since we are only interested in the low-lying spectrum of the system, it is safe to assume that the system is in the ground state in x and y. This assumption makes all calculations effectively 1-dimensional, hence the term *quasi-1-dimensional* or *quasi-1D*.

Assuming the system to be quasi-1D, i.e. effectively reducing the dimensionality of the problem, leads to a considerable reduction in the single-particle basis size. Furthermore, it may increase numerical accuracy, by simplifying the computation of the 6-dimensional integral in V_{ijkl} (see eq. (2.4)). In general, the integral has to be computed numerically, and therefore is a cause of numerical error. If its dimension can be reduced and/or the expression for the integrand can be simplified, the accuracy of the calculations can increase significantly.

Let us have a closer look at how this is done. Assume that the single-particle orbitals can be separated as

$$\phi_i(\mathbf{r}) = \psi_0(x,y)\zeta_i(z) \tag{2.6}$$

where ψ_0 is the ground state in x and y, and ζ_i is the ith eigenstate in z. Then we can write (for simplicity we assume the interaction to be spin-independent)

$$\begin{aligned} V_{ijkl} &= \iint \phi_i^*(\mathbf{r})\phi_j^*(\mathbf{r}')v(\mathbf{r},\mathbf{r}')\phi_k(\mathbf{r})\phi_l(\mathbf{r}')\,\delta_{\sigma_i,\sigma_k}\delta_{\sigma_j,\sigma_l}\,\mathrm{d}\mathbf{r}\,\mathrm{d}\mathbf{r}' \\ &= \iint \mathrm{d}z\mathrm{d}z'\zeta_i^*(z)\zeta_j^*(z')\zeta_k(z)\zeta_l(z')\,\delta_{\sigma_i,\sigma_k}\delta_{\sigma_j,\sigma_l}\times \\ &\qquad \underbrace{\iiiint \mathrm{d}x\mathrm{d}y\mathrm{d}x'\mathrm{d}y'|\psi_0(x,y)|^2|\psi_0(x',y')|^2 v(\mathbf{r},\mathbf{r}')}_{:=V^{\mathrm{eff}}(z,z')} \qquad (2.7) \\ &= \iint \mathrm{d}z\mathrm{d}z'\zeta_i^*(z)\zeta_j^*(z')V^{\mathrm{eff}}(z,z')\zeta_k(z)\zeta_l(z')\,\delta_{\sigma_i,\sigma_k}\delta_{\sigma_j,\sigma_l} \qquad (2.8) \end{aligned}$$

where we have defined the effective interaction in one dimension, V^{eff}. Depending on the form of ψ_0 and v, we may calculate some or all of the integrals in V^{eff} analytically.

In the following, we examine the effective interaction in the two systems considered in this thesis: We discuss to what extent V^{eff} can be determined analytically, what determines ψ_0, the form of v, and which parameters control the effective interaction.

Electrons — For electrons in a semiconductor nanowire we can calculate two integrals in V^{eff} analytically. In this case the ground state $\psi_0(x,y)$ is determined by the transverse confinement potential, which is modelled as a hard-wall cylinder. As to the interaction of electrons, it is the Coulomb interaction. However, the nanowire and its surrounding material (air/substrate) have different dielectric constants, resulting in a screened interaction [53, 74]. The effective screened Coulomb interaction, V_C^{eff}, is derived in appendix A, with the final expression given in eq. (A.17).

Note that in the model we assume a homogeneous material surrounding the nanowire with a *single* dielectric constant ε_{out}, while in reality it is a combination of air, leads, and a Si substrate coated with SiO_2. As the theoretical simulations could be compared with experimental data, ε_{out} was used as a fitting parameter, matching the addition energy (affinity), i.e., the width of the Coulomb diamonds (see section 2.4).

Dipoles — For a gas of ultracold dipolar particles, it turns out that all integrals in V^{eff} can be carried out analytically. Again, ψ_0 is determined by the transverse confinement. For an ultracold atomic or molecular gas, the confinement is typically obtained by a magnetic and/or optical trap, whose potential minimum is in most cases well described by a harmonic potential [2, 9]. We therefore assume that ψ_0 is the ground state of an isotropic two-dimensional harmonic oscillator. The three-dimensional dipole-dipole interaction is given in eq. (1.3). By ignoring the δ-part of the interaction[2], we achieve the effective dipole-dipole interaction

$$V_{\text{dd}}^{\text{eff}}(z-z') = -\frac{d^2(1+3\cos(2\Theta))}{8l_\perp^3}\,\widetilde{V}_{\text{dd}}^{\text{eff}}(|z-z'|/l_\perp) \tag{2.9}$$

where

$$\widetilde{V}_{\text{dd}}^{\text{eff}}(u) = -2u + \sqrt{2\pi}(1+u^2)\,\mathrm{e}^{u^2/2}\,\mathrm{erfc}(u/\sqrt{2})\,. \tag{2.10}$$

Here d^2 is the coupling strength of the dipoles (see section 1.4), Θ is the tilt angle of the dipole moments relative to the z-axis (see figure 1.1(b)), $l_\perp = \sqrt{\hbar/m\omega}$ is the oscillator length in the transverse directions (where ω is the oscillator frequency and m the mass of the particles), and erfc is the complementary error function. The derivation of the above expression can be found in the appendix of ref. [24].

Examples of the effective dipole-dipole interaction between two particles, where one particle is fixed at the origin ($z' = 0$), is given in figure 2.1 for a few values of the dipole tilt angle Θ. At the critical angle, $\Theta_{\text{crit}} = 54.7°$, the interaction is zero. For larger angles, $\Theta > \Theta_{\text{crit}}$, the interaction is repulsive, while for smaller

2 We choose to focus on the effect of the long-range part of the interaction. In an experiment the contact part may be eliminated by Feshbach resonances [9, 18].

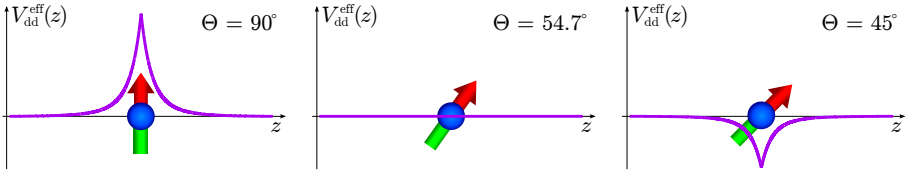

Figure 2.1 The effective dipole-dipole interaction potential, $V_{\rm dd}^{\rm eff}(z - z')$, with one particle fixed at the origin, $z' = 0$, as shown. The flexibility of the interaction depending on the externally tunable dipole tilt angle Θ is evident: The interaction is positive (repulsive) for $\Theta = 90^\circ$ (left panel), zero at the critical angle $\Theta_{\rm crit} = 54.7^\circ$ (centre panel), and negative (attractive) for $\Theta = 45^\circ$ (right panel).

angles, $\Theta < \Theta_{\rm crit}$, the interaction is attractive. This demonstrates how tunable the dipole-dipole interaction is in quasi-1D, while still retaining the stability of the dipolar particles against collapse.

2.1.3 LONGITUDINAL CONFINING POTENTIAL & B-SPLINES

Once the effective interaction, $V^{\rm eff}$, has been determined, the single particle states, $\zeta_i(z)$, in the z-direction are the only ingredient left in order to calculate the interaction integrals V_{ijkl} in eq. (2.8) and create the matrix in the eigenvalue problem (2.5). Assume that the one-body part of the dot Hamiltonian, $\hat{H}_0$, only consists of the kinetic term and the confining potential. As stated at the beginning of this section, it is most natural to choose the single-particle orbitals $\phi_i(\mathbf{r}) = \psi_0(x, y)\zeta_i(z)$ as the one-body eigenstates of $\hat{H}_0$. Therefore, the single-particle orbitals $\zeta_i(z)$ are defined by the longitudinal confining potential. As mentioned in section 1.1, we assume the longitudinal confinement of the particles in the quantum dot to be that of a finite well (see figure 1.2) in all three papers, i.e., the $\zeta_i(z)$ are the wave functions of a one-dimensional finite well, which are well-known[3].

We would also like to be able to model the effects of, for example, defects or disorder in the nanowire quantum dot. These appear as bumps or random fluctuations in the potential. However, the wave function for such potentials is, in general, not

3 That is, the analytic expression for the wave function is known. It depends, however, on the corresponding eigenenergy, which has to be calculated numerically.

known analytically. On the one hand, it is still possible to use the finite-well eigenstates as single-particle basis states, while on the other hand, it can become very hard, in this case, to achieve convergence.

By expanding the single-particle orbitals in *B-splines*, the single-particle orbitals can be approximated numerically for, in principle, any confining potential. The use of B-splines is well-known in atomic and molecular physics [3], but less frequently applied in condensed matter physics. The main advantages, apart from improved convergence when working with non-standard confining potentials, are, firstly, that each B-spline is non-zero on a finite interval only, resulting in finite limits for all integrals involving B-splines. Secondly, the flexibility for obtaining local numerical accuracy is much higher, since in regions where there are abrupt or irregular changes in the confining potential, the density of basis states (B-splines) can be increased in a straightforward manner (by locally increasing the density of break points, see below). Furthermore, numerical integrals may be calculated exactly by Gaussian quadrature.

In what follows, the basics of B-splines and how they are used to solve the one-body Schrödinger equation is briefly described. Given a nondecreasing sequence of *break points*, $\boldsymbol{\tau} = \{\tau_i \,:\, \tau_i \leq \tau_j,\, i < j\}$, the ith B-spline of order k, denoted by $B_{i,k,\boldsymbol{\tau}}$, can be found by the recurrence relation[4]:

$$B_{i,1,\boldsymbol{\tau}}(z) = \begin{cases} 1 & \tau_i < z < \tau_{i+1} \\ 0 & \text{otherwise} \end{cases} \tag{2.11}$$

$$B_{i,k,\boldsymbol{\tau}}(z) = \frac{z - \tau_i}{\tau_{i+k-1} - \tau_i} B_{i,k-1,\boldsymbol{\tau}}(z) + \frac{\tau_{i+k} - z}{\tau_{i+k} - \tau_{i+1}} B_{i+1,k-1,\boldsymbol{\tau}}(z)\,. \tag{2.12}$$

A few examples of B-splines of different order k and for different break point sequences $\boldsymbol{\tau}$ are given in figure 2.2. Some examples of the properties of the B-splines are:

- $B_{i,k,\boldsymbol{\tau}}$ is a polynomial of order $k-1$;

4 B-splines are formally defined by divided differences, see ref. [10].

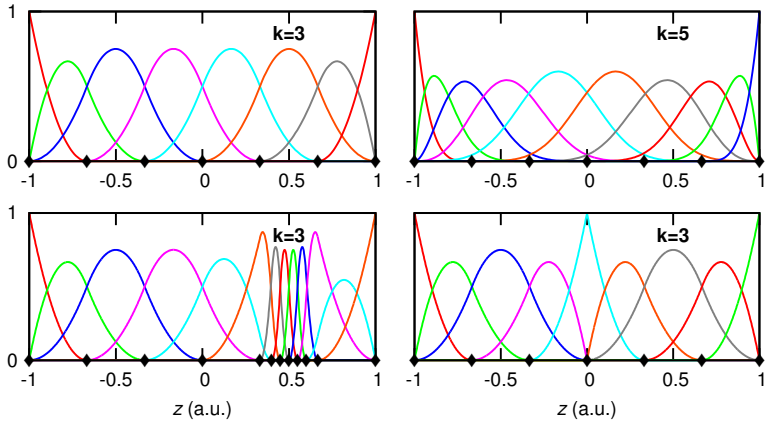

Figure 2.2 Examples of B-spline functions. The order is $k = 3$, except in the top-right panel where $k = 5$. The break points are shown with the symbol ♦. The break points in $z = -1$ and $z = 1$ are k-fold degenerate. All internal break points are simple, except in the bottom-right panel where $z = 0$ is a double break point.

- $B_{i,k,\boldsymbol{\tau}}$ equals zero outside the interval $[\tau_i, \tau_{i+k}]$;
- $B_{i,k,\boldsymbol{\tau}}$ is positive on $]\tau_i, \tau_{i+k}[$;
- $\sum_i B_{i,k,\boldsymbol{\tau}}(z) = 1$ for all z on the interval spanned by $\boldsymbol{\tau}$, provided that the first and last break point is each k-fold degenerate;
- If the function that is to be expanded in terms of $B_{i,k,\boldsymbol{\tau}}$ should have at most m continuous derivatives in a point z, that point should be chosen as a $(k - m - 1)$-fold degenerate break point.

For a mathematically rigorous treatment of B-splines and some more practical properties for computer simulations, e.g. formulae for derivatives, see ref. [10].

Seeking the solutions to the single-particle Schrödinger equation, $\hat{h}|\phi_n\rangle = \epsilon_n|\phi_n\rangle$, we write the single-particle orbitals in terms of the B-splines (here we use the shorthand notation $B_i \equiv B_{i,k,\boldsymbol{\tau}}$),

$$|\phi_n\rangle = \sum_i c_{i,n}|B_i\rangle \,. \tag{2.13}$$

Thus the Schrödinger equation becomes a generalized eigenvalue problem

$$H\mathbf{c}_n = \epsilon_n B\mathbf{c}_n, \tag{2.14}$$

where the eigenvectors $\mathbf{c}_n$ have elements $c_{i,n}$ and the matrix elements of H and B are, respectively,

$$H_{ij} = \langle B_i|\hat{h}|B_j\rangle \quad \text{and} \quad B_{ij} = \langle B_i|B_j\rangle\,. \tag{2.15}$$

By using Gaussian quadrature, the integrals $B_{ij} = \int \mathrm{d}z B_i(z)B_j(z)$ can be calculated exactly. If the confining potential can be expressed as a piecewise polynomial, the integrals in H_{ij} may be calculated exactly as well. Moreover, since B_i is zero outside the interval $[\tau_i, \tau_{i+k}]$, the matrices B and H are $(2k-1)$-diagonal: The only non-zero elements are on the main diagonal and on $k-1$ diagonals on each side of it. For such band matrices, efficient numerical routines exist.

2.2 MODELLING THE LEADS

In contrast to the exhaustive treatment of the quantum dot in the previous section, using a quite detailed description of the system and computationally heavy models, the leads are described in rather simple terms. As is appropriate for metals, the leads are treated within the Fermi liquid theory [41, 48]. That is, we assume the particles in the leads to be noninteracting and replace their mass with an effective mass, depending on the surrounding material. Furthermore, as we did for the quantum dot, we will assume that the leads are quasi-one-dimensional, supporting only one mode (the ground state) in the transversal directions, and that the potential in the leads is constant. In the following we will denote the states in the leads with $k\sigma\ell$, where k is the wave vector, σ the spin, and $\ell = L, R$ denotes the left/right lead.

2.3 TRANSPORT THROUGH A QUANTUM DOT

Finally, we turn our attention to the transport between the leads and quantum dot. The discussion throughout this section is mainly based on refs. [76, 77]. In the Bardeen transfer Hamiltonian method (see eq. (2.1)), the tunneling is described by

$$\hat{H}_{\text{tunneling}} = \sum_{k\sigma\ell,n} \left(t_n(k\sigma\ell)\hat{d}_n^\dagger \hat{c}_{k\sigma\ell} + t_n^*(k\sigma\ell)\hat{c}_{k\sigma\ell}^\dagger \hat{d}_n \right) \tag{2.16}$$

where $t_n(k\sigma\ell)$ are the tunneling couplings between state $k\sigma\ell$ in the leads and the single-particle state n in the quantum dot, $\hat{c}_{k\sigma\ell}^\dagger$ ($\hat{c}_{k\sigma\ell}$) is the creation (annihilation) operator of state $k\sigma\ell$ in the leads, and $\hat{d}_n^\dagger$ ($\hat{d}_n$) is, as before, the creation (annihilation) operator of state n in the quantum dot (note that the spin σ is included in the state label n). The problem at hand is to determine the tunneling couplings $t_n(k\sigma\ell)$, or some expression thereof.

On the other hand, we are interested in the many-body states in the quantum dot. Therefore it is more natural to seek couplings between the leads and many-body states in the dot. First a short note on notation: We adopt the convention that the number of particles increases with the alphabetic order of labels. For example, there is one more particle in state b than in state a, $N_b = N_a + 1$, and similarly $N_c = N_a + 2$, and so on. Now, we insert the unit operators $\sum_a |a\rangle\langle a|$ and $\sum_b |b\rangle\langle b|$ into eq. (2.16) as follows (see appendix A of ref. [64])

$$\begin{aligned}
\hat{H}_{\text{tunneling}} &= \sum_{k\sigma\ell,n} \left(t_n(k\sigma\ell) \sum_b |b\rangle\langle b| \hat{d}_n^\dagger \sum_a |a\rangle\langle a| \hat{c}_{k\sigma\ell} + \text{h.c.} \right) \\
&= \sum_{k\sigma\ell,ab} \Big(\hat{c}_{k\sigma\ell}|b\rangle \underbrace{\sum_n t_n(k\sigma\ell)\langle b|\hat{d}_n^\dagger|a\rangle}_{:=T_{ba}(k\sigma\ell)} \langle a| + \text{h.c.} \Big) \\
&= \sum_{k\sigma\ell,ab} \left(T_{ba}(k\sigma\ell)\hat{c}_{k\sigma\ell}|b\rangle\langle a| + T_{ab}^*(k\sigma\ell)\hat{c}_{k\sigma\ell}^\dagger|a\rangle\langle b| \right) .
\end{aligned} \tag{2.17}$$

In the second step we reordered the terms and defined the scattering amplitude $T_{ba}(k\sigma\ell)$ of a particle in state $k\sigma$ in lead ℓ that tunnels into the dot and thereby

changes its state from a to b. It is straightforward to calculate the overlaps $\langle b|\hat{d}_n^\dagger|a\rangle$ from the many-body states found by the exact diagonalization method. Consequently, once we have determined the tunneling couplings $t_n(k\sigma\ell)$, the amplitudes $T_{ba}(k\sigma\ell)$ are known as well.

2.3.1 PAULI MASTER EQUATION AND FERMI'S GOLDEN RULE

In order to be able to compare our findings with experimental data obtained by transport spectroscopy, we must calculate the current through the system. To that end, there exists a host of different methods of varying complexity and diverse designs, some of which are applicable in combination with a detailed description of the quantum dot. To name a few, there are density matrix approaches such as the 1st order von Neumann (1vN), 2nd order von Neumann (2vN) [64], quantum rate equations [43, 57], generalized master equations [44], and the simplest method of them all, a rate equation [6, 47, 17] also known as (Pauli) master equation. The last one is our method of choice, due to its simplicity.

The Pauli master equation, along with Fermi's golden rule (see below), is valid if the coupling between the leads and quantum dot is weak as compared to the system temperature, $\Gamma \ll k_B T$, where Γ is some average measure of the squared tunneling couplings, $|t_n(k\sigma\ell)|^2$. Furthermore, the level spacing has to be large as compared to the coupling, $\Gamma \ll \Delta\epsilon$. In Paper II, where attractive interaction results in total transport blockade for a finite source-drain bias, V_{sd}, retaining weak coupling Γ is especially important, see further discussion in section 2.3.4.

In the Pauli master equation approach, the current from lead ℓ into the dot is given by

$$I_\ell = e \sum_{ab} \left(R^{\mathrm{in},\ell}_{a\to b} P_a - R^{\mathrm{out},\ell}_{b\to a} P_b \right) \tag{2.18}$$

where the occupation probability P_a of state a in the dot is governed by a classical rate equation[5]

$$\frac{\mathrm{d}P_b}{\mathrm{d}t} = \sum_{a\ell} R^{\mathrm{in},\ell}_{a\to b} P_a + \sum_{c\ell} R^{\mathrm{out},\ell}_{c\to b} P_c - \sum_{c\ell} R^{\mathrm{in},\ell}_{b\to c} P_b - \sum_{a\ell} R^{\mathrm{out},\ell}_{b\to a} P_b \quad (2.19)$$

and $R^{\mathrm{in},\ell}_{a\to b}$ ($R^{\mathrm{out},\ell}_{b\to a}$) is the rate of particle transitions into (out of) the dot from (into) lead ℓ, changing the dot's state from a to b (from b to a).

In addition, we can allow relaxation in the system by adding further transitions to the rate equation above

$$\begin{aligned}\frac{\mathrm{d}P_b}{\mathrm{d}t} = &\sum_{a\ell} \left(R^{\mathrm{in},\ell}_{a\to b} P_a - R^{\mathrm{out},\ell}_{b\to a} P_b \right) + \sum_{c\ell} \left(R^{\mathrm{out},\ell}_{c\to b} P_c - R^{\mathrm{in},\ell}_{b\to c} P_b \right) \\ &+ \sum_{b'} \left(R^{\mathrm{relax}}_{b'\to b} P_{b'} - R^{\mathrm{relax}}_{b\to b'} P_b \right) \end{aligned} \quad (2.20)$$

where the relaxation rates,

$$R^{\mathrm{relax}}_{b\to b'} = \begin{cases} 1/\tau & \text{if } E_{b'} < E_b \\ R^{\mathrm{relax}}_{b'\to b} \mathrm{e}^{-(E_{b'}-E_b)/k_B T} & \text{otherwise,} \end{cases} \quad (2.21)$$

ensure detailed balance[6]. Here τ is the time unit (in the simulations we use $\tau = \hbar/(1\ \mathrm{meV})$).

The rates in eqs. (2.19) and (2.20) are given by

$$\begin{aligned} R^{\mathrm{in},\ell}_{a\to b} &= \Gamma^{\ell}_{ba} f_\ell(E_b - E_a) \\ R^{\mathrm{out},\ell}_{b\to a} &= \Gamma^{\ell}_{ba} \left[1 - f_\ell(E_b - E_a)\right] \end{aligned} \quad (2.22)$$

5 It is implicit in the rate equation that we treat all states in the leads on an equal footing, i.e. we ignore the possibility of different contributions from different states $g \equiv (k\sigma\ell)$ in the leads, since P_a are the diagonal elements of the reduced dot density operator $\hat{\rho}_{\mathrm{dot}} = \mathrm{Tr}_{\mathrm{leads}}[\hat{\rho}]$, $P_a = \sum_g \rho_{ag;ag}$, where $\hat{\rho}$ is the density operator of the system.

6 The condition for detailed balance is $R^{\mathrm{relax}}_{b\to b'} \rho_B(b) = R^{\mathrm{relax}}_{b'\to b} \rho_B(b')$ where ρ_B is the Boltzmann distribution, $\rho_B(b) = \mathrm{e}^{-E_b/k_B T} / \sum_{b'} \mathrm{e}^{-E_{b'}/k_B T}$.

where Γ^{ℓ}_{ba} are the transition rates between states a and b in the dot, and $f_\ell(E) = 1/(\mathrm{e}^{(E-\mu_\ell)/k_BT_\ell}+1)$ is the Fermi-Dirac distribution in lead ℓ with chemical potential[7] μ_ℓ and temperature T_ℓ.

The transition rates Γ^{ℓ}_{ba} are given to first order in the tunneling couplings, by Fermi's golden rule

$$\Gamma^{\ell}_{ba} = \frac{2\pi}{\hbar}\sum_{k\sigma}|T_{ba}(k\sigma\ell)|^2\delta(E_b - E_a - E_k)\,. \tag{2.23}$$

This entails that we only take 1st order tunneling processes into account, i.e. sequential tunneling (one particle tunneling at a time), and that we only take broadening of the quantum dot energy levels due to temperature into account, not the level broadening due to the presence of the leads. Once we have found the tunneling couplings $T_{ba}(k\sigma\ell)$, we can calculate the current I_ℓ.

2.3.2 APPROXIMATING THE TUNNELING COUPLINGS

We will make a series of approximations and assumptions to acquire an expression for the tunneling couplings $T_{ba}(k\sigma\ell)$, and thereby the transition rates Γ^{ℓ}_{ba}. For an overview, see figure 2.3. First of all, since we assume that the quantum dot is quasi-one-dimensional and hence only supports one mode (the ground state) in the transverse directions x, y (see section 2.1.2), we can approximate [76, 77]

$$T_{ba}(k\sigma\ell) \simeq X^{\ell}_{ba}(\sigma)t(k\sigma\ell) \tag{2.24}$$

with

$$X^{\ell}_{ba}(\sigma) = \sum_n \langle b|\hat{d}^\dagger_n|a\rangle\chi^*_n(\sigma)\left[\lambda_n\zeta'_n(z_{\mathrm{i},\ell}) + \zeta_n(z_{\mathrm{i},\ell})\right]^* \tag{2.25}$$

where $\chi_n(\sigma)$ and $\zeta_n(z)$ are the spin and spatial part of the wave function in the quantum dot, respectively, $z_{\mathrm{i},\ell}$ is the interface point of the bands in lead ℓ and the

7 In practice, $\mu_\ell = \mu_{\mathrm{gate}} \pm eV_{\mathrm{sd}}/2$ where e is the elementary charge, μ_{gate} is the gate chemical potential, and V_{sd} is the source-drain bias, see figure 1.2.

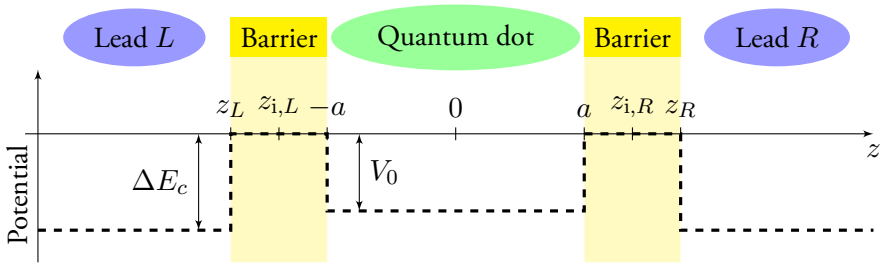

Figure 2.3 Schematic sketch of the system, emphasizing parameters used to model the tunneling between the leads and the quantum dot. The whole system is quasi-one-dimensional; the potential across it is shown with a thick dashed line. The dot potential is a finite well of width $2a$ and depth V_0 (for discussion of other potential shapes, see section 2.1.3), and the lead potential is assumed to be of constant depth ΔE_c. The barriers extend between z_L and $-a$, and a and z_R. We assume that the wave functions in the right (left) lead and the dot intersect at the interface point $z_{\mathrm{i},R}$ ($z_{\mathrm{i},L}$), somewhere in the barrier region (its exact position should not be of importance, so the center of the barrier is a popular choice). Note that the relative width of the barrier region is greatly exaggerated.

quantum dot (see figure 2.3), and $\lambda_n = \hbar/\sqrt{-2m_b\epsilon_n}$ with m_b the effective mass of the particles in the barriers and ϵ_n the single-particle energies in the quantum dot (relative to the barrier height). This, in a sense, separates the states in the dot and the leads.

Inserting eq. (2.24) into eq. (2.23) and rearranging terms, we find

$$\begin{aligned}\Gamma^{\ell}_{ba} &= \sum_{\sigma} |X^{\ell}_{ba}(\sigma)|^2 \underbrace{\frac{2\pi}{\hbar} \sum_{k} |t(k\sigma\ell)|^2 \delta(E_b - E_a - E_k)}_{:=\gamma_{\sigma\ell}(E_b - E_a)} \\ &= \sum_{\sigma} |X^{\ell}_{ba}(\sigma)|^2 \gamma_{\sigma\ell}(E_b - E_a) \end{aligned} \tag{2.26}$$

where we have defined the average coupling strength $\gamma_{\sigma\ell}(E_b - E_a)$. Since we assume the leads to be quasi-one-dimensional as well, and the lead potential to be constant of depth ΔE_c, we arrive at [76, 77]

$$\gamma_{\sigma\ell}(E) \simeq \sqrt{\frac{2(E + \Delta E_c)}{m_\ell}} \frac{\mathrm{e}^{-2|z_{\mathrm{i},\ell} - z_\ell|/\lambda}}{1 - \frac{m_b(E+\Delta E_c)}{m_\ell E}} \tag{2.27}$$

where m_ℓ is the effective mass of the particles in lead ℓ, $\lambda = \hbar/\sqrt{-2m_b E}$, and z_ℓ marks the interface of lead ℓ and the adjoining barrier, see figure 2.3.

2.3.3 TRANSPORT SIMULATION IN PRACTICE

To summarize the transport discussion so far, the rates $R^{\text{in}}_{a\to b}$, $R^{\text{out}}_{b\to a}$ in eq. (2.22) are calculated by using the transition rates Γ^ℓ_{ba} given in eq. (2.26). After having solved the quantum dot system by exact diagonalization (see section 2.1), it is straightforward to calculate the $X^\ell_{ba}(\sigma)$'s from eq. (2.25), while the average couplings $\gamma_{\sigma\ell}(E)$ are given by eq. (2.27).

The transition rates $R^{\text{in}}_{a\to b}$, $R^{\text{out}}_{b\to a}$ are then used to calculate the occupation probabilities P_a, P_b, P_c, etc. by the rate equation (2.19) or (2.20). The rate equation can be set up as a matrix equation[8]

$$\frac{\mathrm{d}}{\mathrm{d}t}\mathbf{P} = J\mathbf{P}\,. \tag{2.28}$$

We seek the steady state solution of the system, $\mathrm{d}\mathbf{P}/\mathrm{d}t = \mathbf{0}$. That is, we wish to find $\mathbf{P}$ such that $J\mathbf{P} = \mathbf{0}$. Thus J must be singular, since otherwise $\mathbf{P} = \mathbf{0}$ is the only solution. More precisely, we need the $n \times n$ matrix J to be of rank $n-1$, in order to get only one solution such that $\sum_i P_i = 1$. Numerically this is not straightforward.

We reformulate the problem[9] by exploiting the condition $\sum_i P_i = 1$, as it implies:

- Once we know all but one P_b, we also know the remaining one.
- If $\mathrm{d}P_b/\mathrm{d}t = 0$ for all but one P_b, then this must also be true for the last remaining one.

8 Note that if one orders the occupation probabilities in $\mathbf{P}$ in order of increasing particle number, J becomes a block matrix that is "tri-block-diagonal", since the occupation probabilities (P_b) only couple to occupations of states with one less (P_a) or one more (P_c) particle, and occupations of states with the same number of particles ($P_{b'}$) in case of relaxation (eq. (2.20)).

9 A. Wacker, private communication.

Consequently, we find the steady state $\mathbf{P}$ by solving the equation

$$\tilde{J}\mathbf{P} = \mathbf{b} \qquad \text{with} \qquad \mathbf{b} = \begin{bmatrix} 0 & 0 & \cdots & 0 & 1 \end{bmatrix}^T \tag{2.29}$$

where

$$\tilde{J} = \begin{bmatrix} J[n-1,n] \\ 1 \quad 1 \quad \cdots \quad 1 \end{bmatrix} = \left\{ \begin{array}{l} \text{the matrix } J \text{ with its last row} \\ \text{substituted by a row of 1's} \end{array} \right\} . \tag{2.30}$$

Ultimately, once we have determined the occupation probabilities $\mathbf{P}$, we use those along with the rates $R^{\text{in}}_{a\to b}$, $R^{\text{out}}_{b\to a}$ to find the current I_ℓ by eq. (2.18).

2.3.4 SECOND ORDER VON NEUMANN METHOD

In Paper II we are especially interested in the regime of weak attractive interaction, where our simulations predict a complete interaction blockade for a finite range of the source-drain bias (V_{sd}). Since only sequencial tunneling is included in the model, a careful analysis of the role of higher order processes, such as cotunneling and pair-tunneling, is needed. To that end, we use the second order von Neumann method (2vN), described in detail in ref. [64], with two levels in the quantum dot.

The second order von Neumann method is, as the name implies, to second order in the squared tunneling couplings, giving level broadening not only due to temperature but also due to the presence of the leads. The main point is, though, that second order processes like pair-tunneling and cotunneling are included in the calculations. This method is computationally much more heavy than the Pauli master equation approach, and at present implementations beyond two dot levels do not exist. However, calculations with two dot levels can indicate the limits of our calculations. Unsurprisingly, the result is that as long as the couplings are so weak that $\Gamma \ll k_B T \ll |U|$, where U is the charging energy, the total current blockade is valid. For stronger couplings, however, the current blockade is broken by higher order tunneling processes.

2.4 CHARGE STABILITY DIAGRAMS

A standard tool in transport spectroscopy is the *charge stability diagram*. This type of diagrams is extensively used in all three papers to give an overview of the theoretical results and to enable comparison with experiments in Paper I. A single charge stability diagram contains a lot of information and may seem quite overwhelming at first sight. The aim of this section is to give a brief description of the main features of charge stability diagrams, especially those used in the papers. A thorough description may be found in ref. [79].

Let us begin by introducing a few terms (see e.g. ref. [31]). The *chemical potential* of a quantum dot with N particles, is given by the energy needed to change the dot from a state a of $N-1$ particles to a state b of N particles

$$\mu_N^{a,b} = E_b - E_a \,. \tag{2.31}$$

The *addition energy* (or *affinity*) for a N-particle dot is given by

$$\Delta\mu_N = \mu_{N+1}^{b_{\rm gs},c_{\rm gs}} - \mu_N^{a_{\rm gs},b_{\rm gs}} \tag{2.32}$$

where the subscript 'gs' denotes the respective ground states. This is the chemical potential needed to add the $(N+1)$st particle to the quantum dot.

The condition for a particle to be able to tunnel into a N-particle quantum dot in state b, and thereby change its state to c, is that the chemical potential $\mu_{N+1}^{b,c}$ of $N+1$ particles is within the potential *bias window* set by the chemical potential of the leads. Expressed in equations,

$$\mu_L > \mu_{N+1}^{b,c} > \mu_R \qquad \text{or} \qquad \mu_L < \mu_{N+1}^{b,c} < \mu_R \,. \tag{2.33}$$

The former condition is depicted in figure 2.4(a). In a similar manner, if a particle is to tunnel out of a N-particle quantum dot in state b, changing it to a $(N-1)$-

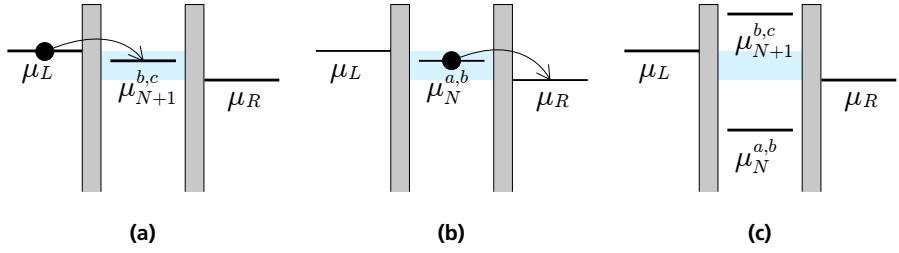

Figure 2.4 Conditions for transport in a N-particle quantum dot in state b. A chemical potential level in the quantum dot must be within the bias window (light blue shaded) for transport to take place. **(a)** A particle can tunnel into the dot, changing its state to c. **(b)** A particle can tunnel out of the dot, changing its state to a. **(c)** No chemical potential level is within the bias window, and hence, transport is blocked.

particle dot in state a, the corresponding N-particle chemical potential must be inside the bias window,

$$\mu_L > \mu_N^{a,b} > \mu_R \qquad \text{or} \qquad \mu_L < \mu_N^{a,b} < \mu_R \tag{2.34}$$

see figure 2.4(b). If neither of these conditions, eqs. (2.33) or (2.34), is fulfilled for any state a or c, no particle can tunnel into or out of the quantum dot: The particle transport is blocked, see figure 2.4(c). For electrons this is the so-called *Coulomb blockade*, while in general the phenomenon is called *interaction blockade* [14].

The size of the bias window is controlled by the source-drain bias, $\mu_L - \mu_R = eV_{\mathrm{sd}}$. Furthermore, the gate potential μ_{gate} determines the position of the chemical potential levels in the dot relative to the chemical potential in the leads:

$$\mu_L = \mu_{\mathrm{gate}} + eV_{\mathrm{sd}}/2 \qquad \text{and} \qquad \mu_R = \mu_{\mathrm{gate}} - eV_{\mathrm{sd}}/2\,. \tag{2.35}$$

In other words, keeping V_{sd} fixed, the gate potential μ_{gate} can be used to "scroll" the chemical potential levels in the quantum dot through the bias window. Now, whenever a chemical potential level, $\mu_N^{a,b}$ or $\mu_{N+1}^{b,c}$, matches either the chemical potential in the left or right lead (see figure 2.6), there will be a jump in the current through the quantum dot. Consequently, a plot of the differential conductance,

$\mathrm{d}I/\mathrm{d}V_{\mathrm{sd}}$, as a function of V_{sd} and μ_{gate} will trace where those jumps occur – that is, map the position of the chemical potential levels in the quantum dot. This map is the charge stability diagram.

The main features of a charge stability diagram are shown in figure 2.5. From the intersection points of the conductance lines, one can infer the relative position of the chemical potential levels in the quantum dot, as explained in figure 2.6. Thus the addition energy (see eq. (2.32)) can be read from the diagram, as shown in figure 2.5(a). Furthermore, we find (the subscript '$i$ex' denotes an ith excited state)

$$\begin{aligned} \mu_N^{a_{\mathrm{gs}},b_{1\mathrm{ex}}} - \mu_N^{a_{\mathrm{gs}},b_{\mathrm{gs}}} &= (E_{b_{1\mathrm{ex}}} - E_{a_{\mathrm{gs}}}) - (E_{b_{\mathrm{gs}}} - E_{a_{\mathrm{gs}}}) \\ &= E_{b_{1\mathrm{ex}}} - E_{b_{\mathrm{gs}}} \equiv \Delta E_N \end{aligned} \tag{2.36}$$

which is the excitation energy of a N-particle quantum dot[10]. Hence, the charge stability diagram directly provides the excitation energies of the quantum dot. This is illustrated in figure 2.5(b). Also, since $\mu_N^{a_{\mathrm{gs}},b} - \mu_N^{a_{\mathrm{gs}},b_{\mathrm{gs}}} = E_b - E_{b_{\mathrm{gs}}}$, one may in principle determine the energy of any N-particle state b relative to the N-particle ground state b_{gs}, from a charge stability diagram.

10 The single-particle excitation energy, or level spacing, is denoted by $\Delta\epsilon$ throughout the thesis, instead of ΔE_1.

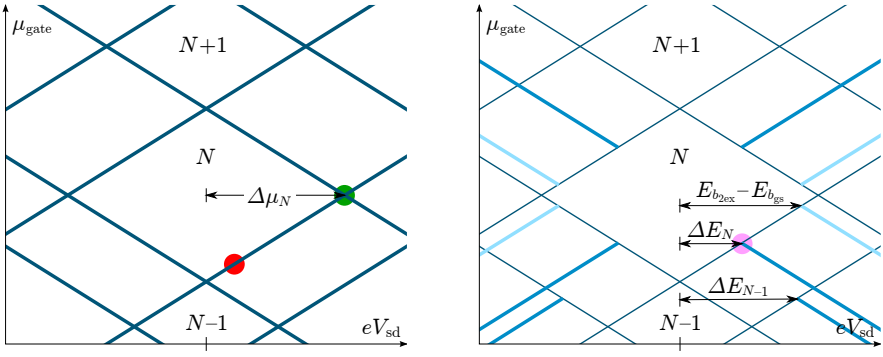

(a) Ground state/ground state tunneling. **(b)** Ground state/excited state tunneling.

Figure 2.5 The main features of a charge stability diagram, showing $\mathrm{d}I/\mathrm{d}V_{\rm sd}$ versus $eV_{\rm sd}$ and $\mu_{\rm gate}$. The red, green and pink dots correspond to the level diagrams in figure 2.6(a), (b), and (c), respectively. **(a)** Tunneling between ground states creates the main conductance lines, that frame the characteristic *Coulomb diamonds* in case of Coulomb interaction, or *interaction blockade diamonds* for a general interaction. The half-width of the Nth diamond provides the addition energy $\Delta\mu_N$, as shown. **(b)** Transitions involving ground and excited states (blue for 1st excited, and light blue for 2nd excited) lead up to or out from the main conductance lines (thin dark blue). Energies of excited states relative to the ground state can be read from the diagram as indicated. (These can also be read from the $\mu_{\rm gate}$-axis, as shown in figure 2 in Paper III.) See further discussion in text and figure 2.6.

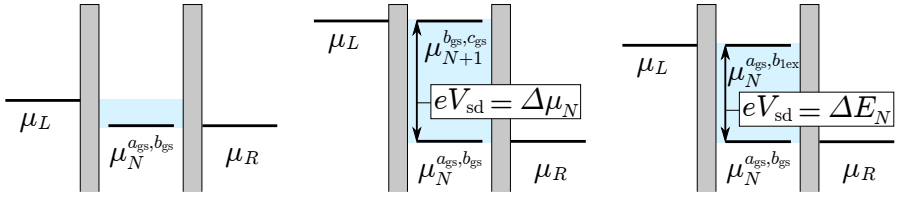

(a) **(b)** **(c)**

Figure 2.6 Alignment of chemical potential levels in the leads and the quantum dot, corresponding to the **(a)** red, **(b)** green, and **(c)** pink dots in figure 2.5. Since $\mu_L - \mu_R = eV_{\rm sd}$, the corresponding differences in quantum dot chemical potentials in (b) and (c) (see eqs. (2.32) and (2.36), respectively) can be read off a charge stability diagram, as shown by arrows in figure 2.5. In other words, the level alignments in (b) provide $eV_{\rm sd} = \mu_L - \mu_R = \mu_{N+1}^{b_{\rm gs},c_{\rm gs}} - \mu_N^{a_{\rm gs},b_{\rm gs}} = \Delta\mu_N$, and in (c) we find $eV_{\rm sd} = \mu_L - \mu_R = \mu_N^{a_{\rm gs},b_{1\rm ex}} - \mu_N^{a_{\rm gs},b_{\rm gs}} = \Delta E_N$.

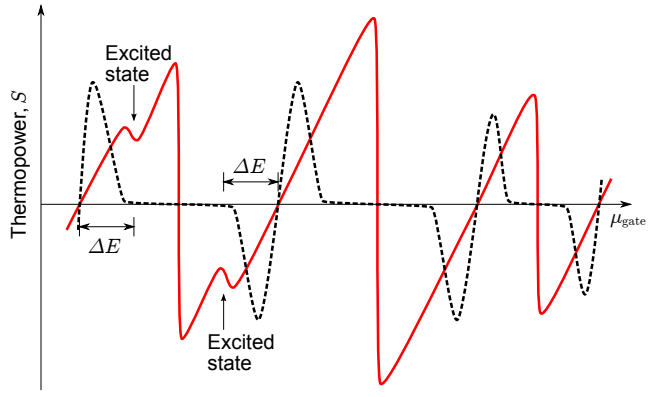

Figure 2.7 Schematic illustration of the thermopower lineshape for sequential tunneling (red solid) and in case cotunneling dominates (black dashed). Excited states appear as fine structure (dips) in the thermopower lineshape, such that the excitation energy ΔE may be deduced, as shown. In case of cotunneling, these signatures of excited states can be lost.

2.5 THERMOPOWER

As mentioned in the Introduction (section 1.5), excited states appear as fine structure in the thermopower lineshape. Thereby, excitation energies may be determined, as shown schematically in figure 2.7. This opens up the possibility to identify the onset of Wigner localization, $\Delta E_2 < \Delta\epsilon$, by thermopower measurements.

In order to calculate the thermopower, S, we set the temperatures of the leads as $T_L = T + \Delta T$ and $T_R = T$ in eq. (2.22), and determine how large a source-drain bias $V_{\rm sd}$ is needed to set the current to zero (in other words, how large a bias is needed to counteract the thermovoltage $V_{\rm th}$ induced by the temperature difference ΔT). Thus we get the thermopower as

$$S = -\frac{V_{\rm th}}{\Delta T} = \left.\frac{V_{\rm sd}}{\Delta T}\right|_{I=0} . \tag{2.37}$$

Note here that the effects of excited states appear in the thermopower at very small source drain bias, $V_{\rm sd}$, that is *within* the Coulomb blockade region. This is in contrast to the conductance, for which the effects of excited states are exponentially

suppressed in the Coulomb blockade region [7], such that they become indistinguishable.

In order to determine the excitation energies from the thermopower, the temperature must be low enough, such that the thermopower fine structure is not smeared out due to thermal broadening. On the other hand, the influence of cotunneling increases at very low temperatures. Cotunneling "cuts" the thermopower [30, 75, 50] as shown schematically in figure 2.7, such that cotunneling can obstruct the signatures of excited states in the thermopower. Consequently, there is a balance to be kept: Low enough temperature to be able to resolve the excited states, but still high enough to suppress cotunneling. Or in other terms, the coupling Γ must be kept low enough to suppress cotunneling, but still high enough in order to deplete the quantum dot.

3

OVERVIEW OF THE PAPERS

3.1 PAPER I – ELECTRONS IN LONG NANOWIRES: WIGNER LOCALIZATION

In this paper we successfully identified the onset of Wigner localization in InSb nanowire quantum dots, both theoretically and experimentally. We simulated InSb nanowires of three different lengths, corresponding to the case of *(i)* independent electrons (70 nm), *(ii)* onset of Wigner localization (160 nm), and *(iii)* Wigner localization (300 nm).

In the first two cases we could compare our findings with experiment, with excellent results for the 160 nm nanowire. There we found the signature $\Delta\epsilon < \Delta E_2$ (see section 1.2) of the onset of Wigner localization for two electrons: Both directly from the energy spectrum (theory), and in the charge stability diagram (experiment; theory for comparison). We could support this observation of the onset of Wigner localization further, by demonstrating the strong suppression of anti-

ferromagnetic coupling (experiment) and the slight spatial separation of the two electrons seen in their density and pair-correlated density (theory).

In the case of a short nanowire (70 nm) we found qualitative agreement between experiment and theory, while a simulation of a 60 nm wire gave better quantitative results (excitation energies). As is pointed out in the paper, the energy bands at the interface of the nanowire and gold contacts are most likely bent (not square shaped as in the model), causing the nanowire to be effectively shorter than 70 nm (the actual contact spacing). One might also suspect that the cause lies in the shortness of the wire, i.e. its length is equal to its diameter, such that the quasi-1D approximation (see section 2.1.2) no longer applies. The discrepancy, however, lies in a too small theoretical value of the single-particle level spacing $\Delta\epsilon$, not too large spacing as would be the result if the quasi-1D approximation was no longer valid.[1]

For a 300 nm long nanowire our simulations showed that full Wigner localization was reached for two electrons. Furthermore, we could identify the onset of Wigner localization for three electrons. Unfortunately we had no successful experiments to compare to in this case, as it proved impossible to process such a long nanowire that was clean enough. That is, instead of a homogeneous potential along the nanowire, it became an effective double dot due to defects[2].

Rashba spin-orbit coupling has been shown to enhance localization of electrons in two-dimensional systems [15, 8, 72]. Spin-orbit coupling is not included in our model, while the effect is considerable in InSb nanowires [60]. Nevertheless, a rough estimate suggests that the spin-orbit coupling in the InSb nanowires considered in the paper (see ref. [61]) should not affect the localization significantly. Proper inclusion of the spin-orbit coupling in our model is, however, necessary to confirm that assessment.

1 A simple calculation also shows, that even for a 70 nm long nanowire we are still well within the quasi-1D approximation.

2 H. A. Nilsson, private communication.

My contribution — I assembled major parts of the numerical code and ran the simulations. I prepared all the figures, except the experimental subfigures. I participated in analysing the results and was the main responsible for the writing of the paper. I did not take part in the experiments.

3.1.1 FURTHER WORK AND OUTLOOK

The good agreement between the simulations and the experiments on InSb nanowire quantum dots felt very encouraging. It was exciting to observe the onset of Wigner localization, but nevertheless, we could not see full Wigner localization in an experiment and were restricted to the analysis of only two particles. We therefore sought new systems, where we might be more successful. One idea was to use InAs-InP heterostructure nanowires, as these could be made thinner than the InSb nanowires at that time (50 nm instead of 70 nm diameter). Hence, one would not need as long a nanowire quantum dot to observe Wigner localization: The simulations indicated that 200 nm would be enough. However, the nanowires bent during growth [29]. Once that obstacle had been overcome, a new one appeared, as the nanowires proved very hard to deplete (obtain no conductance electrons in the dot). In the meantime, we had started thinking of more exotic quantum dots: The clean and highly tunable systems of ultracold dipolar particles in optical traps. The successful transport experiments by Brantut *et al.* [12] were a welcome support to the idea. This led to the following paper, with new interesting findings.

3.2 PAPER II – PARTICLES WITH TUNABLE DIPOLE-INTERACTION: TOTAL CURRENT BLOCKADE

In this letter we studied theoretically a nanowire quantum dot with ultracold dipolar particles. We demonstrated how it is possible, with a single system setup, to cover the regime of Wigner localization, onset of Wigner localization, and even

go to attractive interaction, resulting in total current blockade for a finite range of the source-drain bias.

The tunability of the system is due to the nature of the dipole-dipole interaction, whose strength varies with the tilt angle of the dipoles, Θ (see section 1.4 and figure 2.1). The tilt angle is controlled *externally* by an electric or magnetic field (depending on the dipole type), which allows the exploration of the different interaction regimes within the very same system. Such tunability is, of course, highly appreciated in an experiment, as it makes comparison of the interaction regimes much more reliable.

As we tune the interaction strength, we have to be careful to observe the limitations of our theoretical methods, i.e. the transport formalism (see section 2.3.1), especially with regard to the attractive interaction. Here, we studied transport through a two-level system, including second order tunneling processes by using the 2nd order von Neumann method (2vN). Our conclusion was that the couplings between the reservoirs (leads) and the quantum dot must be sufficiently weak in order to achieve the total current blockade. In other words, if the couplings are not much smaller than the absolute interaction strength, pair-tunneling of particles sets in and breaks the current blockade.

My contribution — I implemented the effective dipole-dipole interaction and ran all the simulations, except for the second order von Neumann calculations. I prepared figures 2 and 3. I was the main responsible for the data analysis and the writing of the paper.

3.3 PAPER III – THERMAL BIAS ACROSS A NANOWIRE: EXCITATION EFFECTS

In this paper we showed how the appearance of excited states as fine structure in the thermopower (Seebeck coefficient) at low temperatures, can be used to identify signatures of the onset of Wigner localization in a quantum dot. The advantage of

thermopower as compared to conventional conductance measurements[3] (such as in Paper I) is that one does not have to apply a high source-drain bias to determine the excitation energies needed. Thereby problems such as stray fields and sample heating can be avoided. However, it is important to keep weak couplings between the leads and dot, as higher order tunneling processes such as cotunneling and pair-tunneling, suppress the thermopower between the Coulomb peaks [30, 75, 50], thereby effectively erasing the signatures of excited states.

At higher temperatures ($3k_BT > \Delta\epsilon$), the thermopower fine structure due to the excited states is smeared out due to thermal broadening. The excited states, however, still affect the thermopower lineshape by suppressing it and shifting its zeroes. This is an important observation, as an unexpected position of the thermopower zeroes might well be misinterpreted as bad data.

My contribution — I implemented the temperature difference in the transport code and improved its accuracy. I performed all the simulations and prepared the figures. I was the main responsible for the data analysis and the writing of the paper.

3.3.1 SCALING OF THERMOCURRENT PEAK HEIGHTS

Some findings never find their way into an article. Here I would like to present one such result that I still feel that deserves not to lie forgotten: An interesting scaling behaviour of the peaks of the thermocurrent.

One issue regarding thermoelectric measurements is that of thermometry: At low temperatures (below 15 K) it has proven hard to measure the temperature of the leads, $T_R = T$ and $T_L = T + \Delta T$, with sufficient accuracy [40]. The question arose, if it is possible to extract information about the temperature of the leads from the thermocurrent (current at zero source-drain bias). By simulating a large

3 Here the question might arise, why the excited states do not appear in the conductance (without thermal bias) at low source-drain bias, if they appear in the thermopower. The answer is that the excited states do affect the conductance in the blockade diamonds, but their effect is exponentially suppressed and, hence, imperceptible [7].

variety of temperature combinations, T and ΔT, we observed a curious result: *The peak height of the thermocurrent is approximately proportional to* $\Delta T/T_{\mathrm{mean}}$*, where* $T_{\mathrm{mean}} = T + \frac{1}{2}\Delta T$ *is the mean temperature of the leads.* This scaling may fail if $\Delta T > T$, and if transport via excited states affects the thermocurrent (generally only at high T_{mean}), as shown in figure 3.1. Note that our calculations only include first order tunneling effects; higher order effects might break this scaling behaviour.

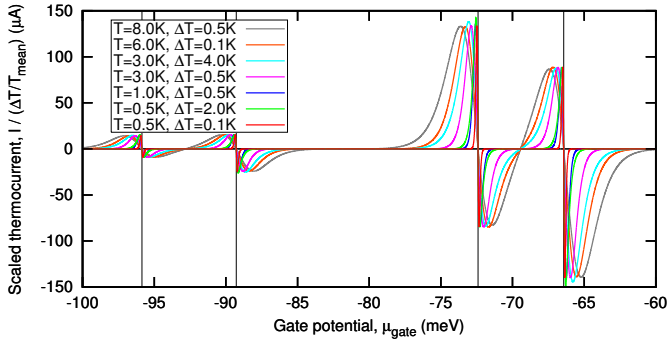

(a) No excited states affect the thermocurrent.

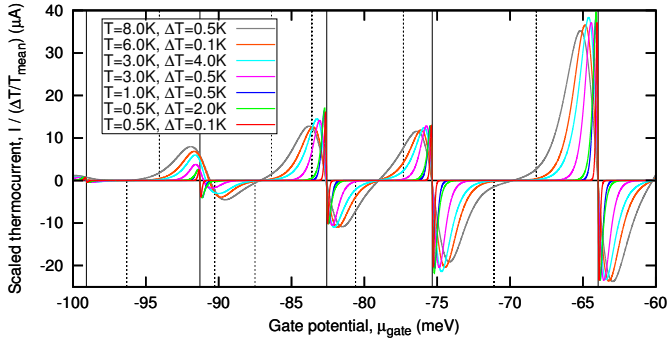

(b) Excited states disturb the peak scaling at high T_{mean}.

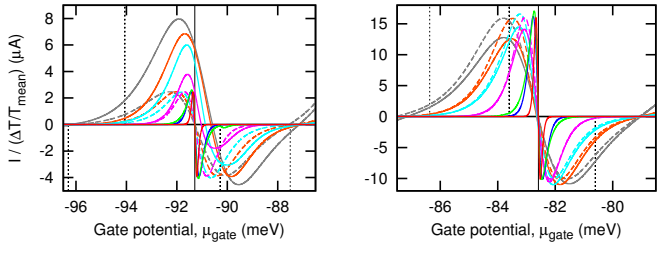

(c) 2nd and 3rd peak pair of **(b)**. Dashed curves correspond to calculations excluding excited states.

Figure 3.1 Scaled thermocurrent in an InSb nanowire quantum dot. The heights of the current peaks scale approximately as $\Delta T/T_{\mathrm{mean}}$. Deviations from this scaling behaviour occur in the case $\Delta T > T$ (green and light blue) and at high T_{mean} if excited states affect the thermocurrent. The thin vertical lines show the chemical potentials in the quantum dot involving ground states (solid) and excited states (dotted). **(a)** Short nanowire: No excited states affect the thermocurrent. **(b)** Long nanowire: Excited states disturb the scaling of the thermocurrent peaks at high T_{mean}. **(c)** A closer look at the 2nd and 3rd current peak pairs in (b). If excited states are excluded in the calculations (dashed curves), the scaling of the thermocurrent peaks is restored as long as $\Delta T < T$.

4

DOUBLE QUANTUM DOT: PRELIMINARY RESULTS

Serially coupled quantum dots are an active area of research. Those are realized, for example, in heterostructure or finger-gated semiconductor nanowires [35, 32], or in optical lattices [9]. The use of B-splines (section 2.1.3) enables us to investigate such systems. In this chapter, the simplest case of coupled quantum dots – a double quantum dot – is considered. Preliminary results on the possible reversal of the odd-even size staggering of Coulomb diamonds in double-well nanowire quantum dots, are presented. The parameters used correspond to an InSb nanowire of diameter 70 nm, but the results are general in nature.

4.1 REVERSAL OF THE ODD-EVEN SIZE STAGGERING OF THE COULOMB DIAMONDS

As described in section 2.4, the half-width of the Coulomb diamonds provides the charging energy, i.e., the potential energy needed to add another particle into the quantum dot. In absence of very strong interaction, an odd-even size staggering of the Coulomb diamonds is common in quasi-one-dimensional quantum dots [65]. That is, the diamonds corresponding to an even number of particles N in the dot are larger than the neighbouring diamonds for odd N. This can be understood from a constant interaction model: Many-body states are built by adding spin-half particles into single-particle levels. Adding an *even* particle such that $N = 2n - 1$ becomes $N = 2n$, an already occupied single-particle level is filled, and thus only the interaction energy has to be overcome. Adding an *odd* particle such that $N = 2n$ becomes $N = 2n + 1$, on the other hand, requires adding a particle to a new single-particle level that is higher in energy, and hence, it is required to both overcome the interaction energy and the energy difference between adjacent single-particle levels. Therefore, a larger chemical potential is needed to add odd particles to the quantum dot than even particles. Hence, the size of the even N Coulomb diamonds is generally larger than that of the odd N diamonds.

Let us now consider two serially coupled quantum dots in quasi-one dimension, where one dot is considerably smaller than the other. The double dot can be represented by a double-well confining potential, such as shown in the top right panel of figure 4.1. We continue the discussion in terms of the constant interaction model. The single-particle energy levels of the smaller dot will be higher in energy and with a larger level spacing than the energy levels of the larger dot. Starting to load particles into the double dot, it is therefore to be expected that the particles will first populate the larger dot. However, the balance of the interaction within each dot and between the two dots must be considered as well. The interaction within the larger dot is weaker than that within the smaller dot, whereas the magnitude of the interaction relative to the kinetic energy is greater in the larger dot. At some point, the lowest level in the smaller dot is reached. Due to the larger interaction

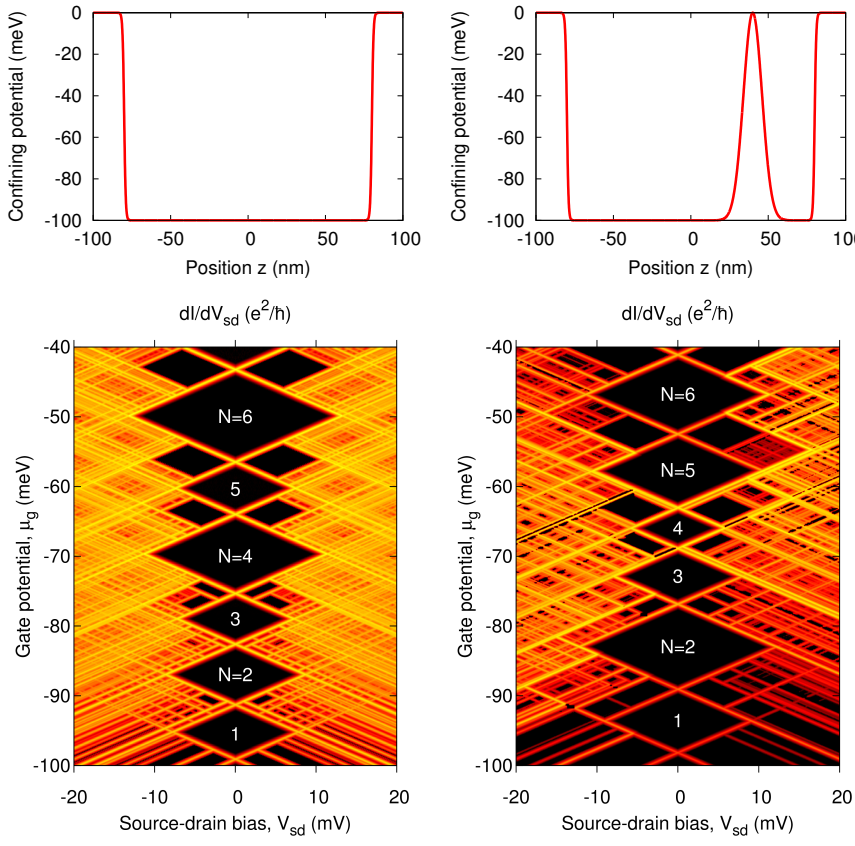

Figure 4.1 Upper panel: Confining potential of a single quantum dot of length $L = 160$ nm (left) and a double quantum dot (right). The double dot is made by adding a gaussian peak to the finite well confining potential of the single dot. The peak is located at $z = 40$ nm and is of height 100 meV and width $\mathrm{FWHM} = 20$ nm. Lower panel: Charge stability diagram for the single (left) and double (right) quantum dot. Note that the odd-even size staggering of the Coulomb diamonds is temporarily reversed for $N = 4$ and $N = 5$ in the double dot.

in the smaller dot, the next particle entering the system might occupy the larger dot instead of filling the energy level in the smaller dot. Thus the odd-even size staggering of the Coulomb diamonds will be temporarily reversed, until the energy level in the smaller dot is filled. This phenomenon is evident in figure 4.1, where the size of the $N = 4$ and $N = 5$ diamonds is swapped, when a single-well confining potential is turned into a double-well potential.

The above analysis is further confirmed by the ground state probability densities of the double dot, shown in the upper panel of figure 4.2. To assist with the interpretation of the probability density in the larger dot, the probability density of a corresponding (single) quantum dot is shown in the lower panel of the figure. For up to three particles, the probability density in the small dot is zero. The possibility of occupying the small dot only arises when the fourth particle is added to the system (the area under the density peak in the small dot is $A_{\mathrm{small}} = 0.68$ for $N = 4$). For five particles, there is one particle in the smaller dot ($A_{\mathrm{small}} = 1.00$ for $N = 5$) and the probability density in the larger dot agrees with that of $N = 4$ in the corresponding single dot. When the sixth particle enters the system, there are two particles in the smaller dot ($A_{\mathrm{small}} = 2.00$ for $N \geq 6$ and the probability density in the larger dot hardly changes), turning the odd-even size staggering back to normal. Subsequently, as the seventh and eighth particles are added, the probability density remains unchanged in the small dot, while the probability density in the large dot resembles that of $N = 5$ and $N = 6$ in the corresponding single dot.

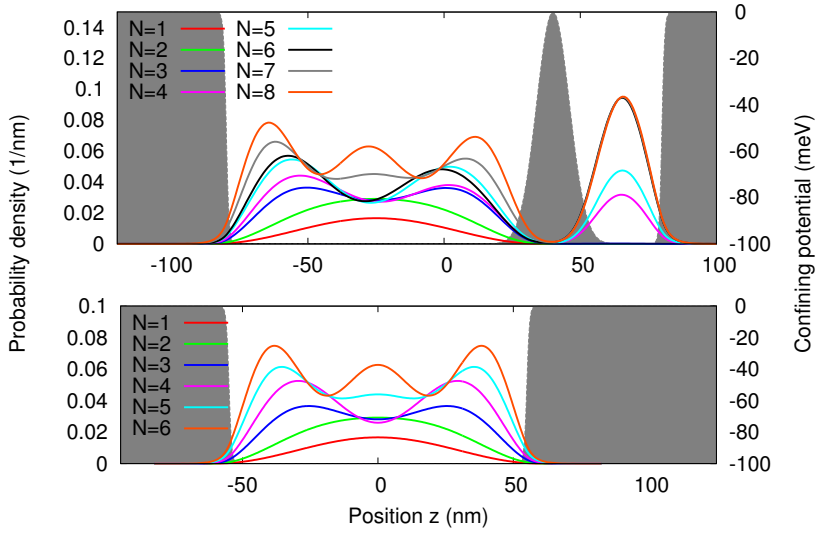

Figure 4.2 Upper panel: Probability density in the double quantum dot presented in the right half of figure 4.1. Lower panel: To help with the interpretation of the probability density in the larger dot, the probability density of a corresponding single quantum dot ($L = 110$ nm) is shown. The confining potential is depicted as a gray-shaded background in both panels.

5

OUTLOOK

Quantum dots provide a rich playfield for investigating many-body physics at the quantum level [65, 9]. We have come a long way, both in our theoretical understanding and experimental control of such systems, e.g. in semiconductors and ultracold gases. However, there are always new questions to be answered, new directions to take. Experimental techniques are refined and novel approaches arise. Computers can handle ever larger calculations, and theoretical models and computational methods are under constant development.

The model described in the thesis is quite versatile, regarding e.g. the type of particles, interaction, and transverse confining potential, and can, as such, be used to describe many new systems. Most importantly, the model can be extended and improved. An arbitrary longitudinal potential in the quantum dot has already been implemented. An interesting example of employing this new feature, is to investigate the effect of disorder on the thermopower in interacting ultracold gases [11].

Another example of a non-constant confining potential, is to look into serially coupled double quantum dots, such as discussed in chapter 4. A quite interesting beating pattern has been observed in the conductance and thermopower of double semiconductor quantum dots [28]. Here a smaller quantum dot provides an overlaying Coulomb diamond pattern on top of the Coulomb diamonds of the larger quantum dot, in addition to a slow modulation of the thermopower imposed on a more narrow pattern by the larger dot. Furthermore, going beyond the double dot would be an exciting possibility. For example, looking into periodic structures, such as in one-dimensional optical lattices [9].

As discussed in section 2.5, higher order tunneling processes become prominent in the thermopower at low temperatures and/or larger couplings. Including second order tunneling processes by the second order von Neumann method [64] would, therefore, substantially increase the applicability of the model. This is especially important if thermopower is applied as a characterization tool for nanowire quantum dots. In that case, theoretical understanding of the eperimental data is essential. Here, our model provides the strong interaction perspective.

Finally, including spin-orbit coupling could strengthen the model. Both semiconductor quantum dots [33, 61] and atomic gases [42] can exhibit significant spin-orbit coupling, leading to interesting effects, such as the enhancement of Wigner localization [15].

A

EFFECTIVE SCREENED COULOMB INTERACTION

Consider a cylindrical nanowire of radius R and dielectric constant ε_{in}, submerged in a medium of dielectric constant ε_{out}, see figure A.1. The aim of this appendix is to find the effective one-dimensional interaction of electrons along the nanowire, valid in the quasi-1D approximation (see section 2.1.2). Thus we assume that the wave function of the system separates

$$\phi_i(\mathbf{r}) = \psi_0(x, y)\zeta_i(z) \tag{A.1}$$

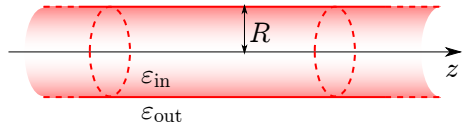

Figure A.1 Cylindrical nanowire of radius R and dielectric constant ε_{in}. The surrounding medium has dielectric constant ε_{out}.

where ψ_0 is the ground state in the transverse directions and ζ_i is the ith single-particle orbital. Accordingly, as defined in eq. (2.7), the effective interaction between two electrons at positions z_1 and z_2, respectively, is given by

$$V_C^{\text{eff}}(z_1, z_2) = \iiiint \mathrm{d}x_1 \mathrm{d}y_1 \mathrm{d}x_2 \mathrm{d}y_2 |\psi_0(x_1, y_1)|^2 |\psi_0(x_2, y_2)|^2 v_C(\mathbf{r}_1, \mathbf{r}_2) \tag{A.2}$$

where $v_C(\mathbf{r}_1, \mathbf{r}_2)$ is the interaction of the electrons in three dimensions.

In cylindrical coordinates, the ground state of a hard-wall cylinder of radius R is

$$\psi_0(\rho, \varphi) = \begin{cases} \frac{1}{\sqrt{2\pi} N_0} J_0(k_0 \rho) & \rho \leq R \\ 0 & \rho > R \end{cases} \tag{A.3}$$

where N_0 is a normalization constant, J_0 is the zeroth order Bessel function of the first kind, $k_0 R$ is the lowest zero of J_0, and $E_0 = \hbar^2 k_0^2 / 2m$ is the ground state energy, with m the effective mass of the electrons. The screened interaction of the electrons in the nanowire is given by [53, 74]

$$v_C(\mathbf{r}_1, \mathbf{r}_2) = v_{\text{unscr}}(\mathbf{r}_1, \mathbf{r}_2) + v_{\text{corr}}(\mathbf{r}_1, \mathbf{r}_2) \tag{A.4}$$

where

$$\begin{aligned} v_{\text{unscr}}(\mathbf{r}_1, \mathbf{r}_2) &= \frac{e^2}{4\pi\varepsilon_{\text{in}}} \frac{1}{|\mathbf{r}_1 - \mathbf{r}_2|} \\ &= \frac{e^2}{4\pi\varepsilon_{\text{in}}} \frac{1}{\sqrt{\rho_1^2 + \rho_2^2 - \rho_1 \rho_2 \cos(\varphi_1 - \varphi_2) + (z_1 - z_2)^2}} \end{aligned} \tag{A.5}$$

is the familiar unscreened Coulomb interaction with e the elementary charge, and

$$\begin{aligned} v_{\text{corr}}(\mathbf{r}_1, \mathbf{r}_2) = -\frac{e^2}{2\pi^2 \varepsilon_{\text{in}}} \sum_{\alpha=-\infty}^{\infty} \int_0^\infty \mathrm{d}k \Bigg[& \mathrm{e}^{\mathrm{i}\alpha(\varphi_1 - \varphi_2)} \cos(k(z_1 - z_2)) \\ & \times f_\alpha\left(\frac{\varepsilon_{\text{in}}}{\varepsilon_{\text{out}}}, kR\right) I_\alpha(k\rho_1) I_\alpha(k\rho_2) \Bigg] \end{aligned} \tag{A.6}$$

is a correction to the Coulomb interaction due to the different dielectric constants of the wire and the surrounding material, with

$$f_\alpha\left(\frac{\varepsilon_{\rm in}}{\varepsilon_{\rm out}}, kR\right) = \frac{(1-\frac{\varepsilon_{\rm in}}{\varepsilon_{\rm out}})K_\alpha(kR)K'_\alpha(kR)}{I_\alpha(kR)K'_\alpha(kR) - \frac{\varepsilon_{\rm in}}{\varepsilon_{\rm out}}I'_\alpha(kR)K_\alpha(kR)}\,. \tag{A.7}$$

Here I_α and K_α are the modified Bessel functions of the first and second kind, respectively, and I'_α and K'_α are their derivatives.

Let us separate the effective interaction in an analogous manner to the two terms in $v_C(\mathbf{r}_1, \mathbf{r}_2)$,

$$V_C^{\rm eff}(z_1, z_2) = V_{\rm unscr}^{\rm eff}(z_1, z_2) + V_{\rm corr}^{\rm eff}(z_1, z_2)\,. \tag{A.8}$$

The effective unscreened Coulomb interaction is thus

$$\begin{aligned} &V_{\rm unscr}^{\rm eff}(z_1, z_2) \\ &\quad = \iiiint \mathrm{d}\rho_1\mathrm{d}\rho_2\mathrm{d}\varphi_1\mathrm{d}\varphi_2\rho_1\rho_2|\psi_0(\rho_1,\varphi_1)|^2|\psi_0(\rho_2,\varphi_2)|^2 v_{\rm unscr}(\mathbf{r}_1,\mathbf{r}_2) \\ &\quad = \frac{e^2}{4\pi\varepsilon_{\rm in}}\frac{1}{4\pi^2N_0^4}\int_0^R \mathrm{d}\rho_1\int_0^R \mathrm{d}\rho_2\int_0^{2\pi}\mathrm{d}\varphi_1\int_0^{2\pi}\mathrm{d}\varphi_2 \\ &\qquad\qquad \times \frac{\rho_1\rho_2|J_0(k_0\rho_1)|^2|J_0(k_0\rho_2)|^2}{\sqrt{\rho_1^2+\rho_2^2-\rho_1\rho_2\cos(\varphi_1-\varphi_2)+(z_1-z_2)^2}}\,. \end{aligned} \tag{A.9}$$

We make the following change of variables

$$\begin{aligned} k_0\rho_1 &= k_0Rr_1 = \kappa_0 r_1 \\ k_0\rho_2 &= k_0Rr_2 = \kappa_0 r_2 \end{aligned}\,, \qquad \begin{aligned} \bar\varphi &= \tfrac{1}{2}(\varphi_1+\varphi_2) \\ \varphi &= \varphi_1-\varphi_2 \end{aligned}\,, \qquad z = z_1 - z_2 \tag{A.10}$$

and note especially that due to the identity $\cos(\theta) = \cos(2\pi - \theta)$, the integration limits for $\bar{\varphi}$ and φ can both be set to $[0, 2\pi]$. Hence, the integral over $\bar{\varphi}$ simply equals 2π, and we arrive at

$$V_{\mathrm{unscr}}^{\mathrm{eff}}(z) = \frac{e^2}{4\pi\varepsilon_{\mathrm{in}}} \frac{R^3}{2\pi N_0^4} \int_0^{2\pi} \mathrm{d}\varphi \int_0^1 \mathrm{d}r_1 \int_0^1 \mathrm{d}r_2 \frac{r_1 |J_0(\kappa_0 r_1)|^2 r_2 |J_0(\kappa_0 r_2)|^2}{\sqrt{r_1^2 + r_2^2 - 2r_1 r_2 \cos\varphi + (z/R)^2}} \,. \tag{A.11}$$

For the effective correction term we find

$$\begin{aligned}
V_{\mathrm{corr}}^{\mathrm{eff}}(z_1, z_2) &= \iiiint \mathrm{d}\rho_1 \mathrm{d}\rho_2 \mathrm{d}\varphi_1 \mathrm{d}\varphi_2 \rho_1 \rho_2 |\psi_0(\rho_1, \varphi_1)|^2 |\psi_0(\rho_2, \varphi_2)|^2 v_{\mathrm{corr}}(\mathbf{r}_1, \mathbf{r}_2) \\
&= -\frac{e^2}{2\pi^2 \varepsilon_{\mathrm{in}}} \frac{1}{4\pi^2 N_0^4} \int_0^R \mathrm{d}\rho_1 \int_0^R \mathrm{d}\rho_2 \int_0^{2\pi} \mathrm{d}\varphi_1 \int_0^{2\pi} \mathrm{d}\varphi_2 \\
&\quad \times \rho_1 \rho_2 |J_0(k_0 \rho_1)|^2 |J_0(k_0 \rho_2)|^2 \\
&\quad \times \Bigg(\sum_{\alpha=-\infty}^{\infty} \int_0^{\infty} \mathrm{d}k \Big[\mathrm{e}^{\mathrm{i}\alpha(\varphi_1 - \varphi_2)} \cos(k(z_1 - z_2)) \\
&\qquad \times f_\alpha \left(\tfrac{\varepsilon_{\mathrm{in}}}{\varepsilon_{\mathrm{out}}}, kR \right) I_\alpha(k\rho_1) I_\alpha(k\rho_2) \Big] \Bigg) \\
&= -\frac{e^2}{2\pi^2 \varepsilon_{\mathrm{in}}} \frac{1}{4\pi^2 N_0^4} \sum_{\alpha=-\infty}^{\infty} \int_0^{2\pi} \mathrm{d}\varphi_1 \, \mathrm{e}^{\mathrm{i}\alpha\varphi_1} \int_0^{2\pi} \mathrm{d}\varphi_2 \, \mathrm{e}^{-\mathrm{i}\alpha\varphi_2} \\
&\quad \times \int_0^{\infty} \mathrm{d}k \left(\cos(k(z_1 - z_2)) f_\alpha \left(\tfrac{\varepsilon_{\mathrm{in}}}{\varepsilon_{\mathrm{out}}}, kR \right) \right. \\
&\qquad \left. \times \left[\int_0^R \mathrm{d}\rho \, \rho |J_0(k_0 \rho)|^2 I_\alpha(k\rho) \right]^2 \right)
\end{aligned} \tag{A.12}$$

where we have exploited that the integrals over ρ_1 and ρ_2 are identical and therefore renamed the integration variables ρ_1, ρ_2 as ρ. Now, note that the integrals over φ_1 and φ_2 are identically zero unless $\alpha = 0$, in which case the integrals equal 2π.

Hence, the sum disappears and only terms with $\alpha = 0$ remain in the integral. We make the following variable substitution

$$\begin{aligned} k\rho &= kRr = \kappa r \\ k_0\rho &= k_0 Rr = \kappa_0 r \end{aligned}, \qquad z = z_1 - z_2 \tag{A.13}$$

and by inserting f_0 from eq. (A.7) we thus find

$$\begin{aligned} &V_{\mathrm{corr}}^{\mathrm{eff}}(z) \\ &\quad = -\frac{e^2}{2\pi^2\varepsilon_{\mathrm{in}}}\frac{R^3}{N_0^4}\int_0^\infty \mathrm{d}\kappa \left(\cos(\kappa\tfrac{z}{R})\frac{(1-\frac{\varepsilon_{\mathrm{in}}}{\varepsilon_{\mathrm{out}}})K_0(\kappa)K_0'(\kappa)}{I_0(\kappa)K_0'(\kappa) - \frac{\varepsilon_{\mathrm{in}}}{\varepsilon_{\mathrm{out}}}I_0'(\kappa)K_0(\kappa)}\right. \\ &\qquad\qquad \left. \times \left[\int_0^1 \mathrm{d}r\, r|J_0(\kappa_0 r)|^2 I_0(\kappa r)\right]^2\right) \\ &\quad = \frac{e^2}{4\pi\varepsilon_{\mathrm{in}}}\frac{2R^3}{\pi N_0^4}\left(\frac{\varepsilon_{\mathrm{in}}}{\varepsilon_{\mathrm{out}}} - 1\right)\int_0^\infty \mathrm{d}\kappa \left(\frac{\cos(\kappa\frac{z}{R})K_0(\kappa)K_1(\kappa)}{I_0(\kappa)K_1(\kappa) + \frac{\varepsilon_{\mathrm{in}}}{\varepsilon_{\mathrm{out}}}I_1(\kappa)K_0(\kappa)}\right. \\ &\qquad\qquad \left. \times \left[\int_0^1 \mathrm{d}r\, r|J_0(\kappa_0 r)|^2 I_0(\kappa r)\right]^2\right) \end{aligned} \tag{A.14}$$

where we have used the identities $I_0'(\kappa) = I_1(\kappa)$ and $K_0'(\kappa) = -K_1(\kappa)$, see eq. (9.6.27) in ref. [62]. Due to the exponentially asymptotic behaviour of the modified Bessel functions, it is often better to use the scaled modified Bessel functions

$$\widetilde{I}_n(\kappa) = \mathrm{e}^{-|\kappa|}\, I_n(\kappa), \qquad \widetilde{K}_n(\kappa) = \mathrm{e}^{\kappa}\, K_n(\kappa) \tag{A.15}$$

in numerical calculations. Finally, we arrive at

$$\begin{aligned} V_{\mathrm{corr}}^{\mathrm{eff}}(z) = \frac{e^2}{4\pi\varepsilon_{\mathrm{in}}}\frac{2R^3}{\pi N_0^4}\left(\frac{\varepsilon_{\mathrm{in}}}{\varepsilon_{\mathrm{out}}} - 1\right)\int_0^\infty \mathrm{d}\kappa \left(\frac{\cos(\kappa\frac{z}{R})}{\widetilde{I}_0(\kappa)\widetilde{K}_1(\kappa) + \frac{\varepsilon_{\mathrm{in}}}{\varepsilon_{\mathrm{out}}}\widetilde{I}_1(\kappa)\widetilde{K}_0(\kappa)}\right. \\ \left. \times \left[\int_0^1 \mathrm{d}r\, r|J_0(\kappa_0 r)|^2 \widetilde{I}_0(\kappa r)\sqrt{\widetilde{K}_0(\kappa)\widetilde{K}_1(\kappa)}\,\mathrm{e}^{-\kappa(1-r)}\right]^2\right). \end{aligned} \tag{A.16}$$

In summary, the effective screened Coulomb interaction of two electrons separated by a distance z in a quasi one-dimensional cylindrical nanowire of radius R and dielectric constant ε_{in}, submerged in a medium of dielectric constant ε_{out} (see figure A.1), is given by

$$\begin{aligned} V_C^{\text{eff}}(z) \\ &= \frac{e^2}{4\pi\varepsilon_{\text{in}}} \frac{R^3}{2\pi N_0^4} \int_0^{2\pi} \mathrm{d}\varphi \int_0^1 \mathrm{d}r_1 \int_0^1 \mathrm{d}r_2 \frac{r_1 |J_0(\kappa_0 r_1)|^2 r_2 |J_0(\kappa_0 r_2)|^2}{\sqrt{r_1^2 + r_2^2 - 2r_1 r_2 \cos\varphi + (z/R)^2}} \\ &\quad + \frac{e^2}{4\pi\varepsilon_{\text{in}}} \frac{2R^3}{\pi N_0^4} \left(\tfrac{\varepsilon_{\text{in}}}{\varepsilon_{\text{out}}} - 1 \right) \int_0^\infty \mathrm{d}\kappa \left(\frac{\cos(\kappa \frac{z}{R})}{\widetilde{I}_0(\kappa)\widetilde{K}_1(\kappa) + \frac{\varepsilon_{\text{in}}}{\varepsilon_{\text{out}}} \widetilde{I}_1(\kappa)\widetilde{K}_0(\kappa)} \right. \\ &\qquad \left. \times \left[\int_0^1 \mathrm{d}r\, r |J_0(\kappa_0 r)|^2 \widetilde{I}_0(\kappa r) \sqrt{\widetilde{K}_0(\kappa)\widetilde{K}_1(\kappa)}\, \mathrm{e}^{-\kappa(1-r)} \right]^2 \right) \end{aligned} \tag{A.17}$$

where

$J_0(x)$	is the zeroth order Bessel function of the first kind,
$\kappa_0 = k_0 R$	is the lowest zero of J_0,
N_0	is the normalization constant of J_0,
$\widetilde{I}_n(x), \widetilde{K}_n(x)$	are the nth order scaled modified Bessel functions of the first and second kind, respectively.

REFERENCES

[1] Aikawa, K., Frisch, A., Mark, M., Baier, S., Grimm, R., and Ferlaino, F., "Reaching Fermi degeneracy via universal dipolar scattering," Physical Review Letters **112**, 010404 (2014).

[2] Anderson, M. H., Ensher, J. R., Matthews, M. R., Wieman, C. E., and Cornell, E. A., "Observation of Bose-Einstein Condensation in a Dilute Atomic Vapor," Science **269**, 198 (1995).

[3] Bachau, H., Cormier, E., Decleva, P., Hansen, J. E., and Martín, F., "Applications of B-splines in atomic and molecular physics," Reports on Progress in Physics **64**, 1815 (2001).

[4] Baranov, M. A., "Theoretical progress in many-body physics with ultracold dipolar gases," Physics Reports **464**, 71 (2008).

[5] Bardeen, J., "Tunnelling from a many-particle point of view," Physical Review Letters **6**, 57 (1961).

[6] Beenakker, C. W. J., "Theory of Coulomb-blockade oscillations in the conductance of a quantum dot," Physical Review B **44**, 1646 (1991).

[7] Beenakker, C. W. J. and Staring, A. A. M., "Theory of the thermopower of a quantum dot," Physical Review B **46**, 9667 (1992).

[8] Berg, E., Rudner, M. S., and Kivelson, S. A., "Electronic liquid crystalline phases in a spin-orbit coupled two-dimensional electron gas," Physical Review B **85**, 035116 (2012).

[9] Bloch, I., Dalibard, J., and Zwerger, W., "Many-body physics with ultracold gases," Reviews of Modern Physics **80**, 885 (2008).

[10] de Boor, C., *A Practical Guide to Splines* (Springer-Verlag, New York, 1978).

[11] Brantut, J.-P., Grenier, C., Meineke, J., Stadler, D., Krinner, S., Kollath, C., Esslinger, T., and Georges, A., "A Thermoelectric Heat Engine with Ultracold Atoms," Science **342**, 713 (2013).

[12] Brantut, J.-P., Meineke, J., Stadler, D., Krinner, S., and Esslinger, T., "Conduction of Ultracold Fermions Through a Mesoscopic Channel," Science **337**, 1069 (2012).

[13] Caneva, K. L., "Ørsted's Presentation Of Others'—And His Own—Work," in *Hans Christian Ørsted And The Romantic Legacy In Science*, Boston Studies In The Philosophy Of Science, Vol. 241, edited by R. M. Brain, R. S. Cohen, and O. Knudsen (Springer Netherlands, 2007) pp. 273–338.

[14] Capelle, K., Borgh, M., Kärkkäinen, K., and Reimann, S. M., "Energy Gaps and Interaction Blockade in Confined Quantum Systems," Physical Review Letters **99**, 010402 (2007).

[15] Cavalli, A., Malet, F., Cremon, J. C., and Reimann, S. M., "Spin-orbit-enhanced Wigner localization in quantum dots," Physical Review B **84**, 235117 (2011).

[16] Chakraborty, T., *Quantum Dots: A Survey of the Properties of Artificial Atoms* (Elsevier Science, 1999).

[17] Chen, G., Klimeck, G., Datta, S., Chen, G., and Goddard III, W. A., "Resonant tunneling through quantum-dot arrays," Physical Review B **50**, 8035 (1994).

[18] Chin, C., Grimm, R., Julienne, P., and Tiesinga, E., "Feshbach resonances in ultracold gases," Reviews of Modern Physics **82**, 1225 (2010).

[19] Cramer, C. J., *Essentials of Computational Chemistry*, 2nd ed. (John Wiley & Sons Ltd, 2004) pp. 199–204.

[20] Cremon, J. C., *Quantum few-body physics with the configuration interaction approach – Method development and application to physical systems*, Ph.D. thesis, Lund University (2010).

[21] Cremon, J. C., Bruun, G. M., and Reimann, S. M., "Tunable Wigner States with Dipolar Atoms and Molecules," Physical Review Letters **105**, 255301 (2010).

[22] Datta, S., *Electronic Transport in Mesoscopic Systems* (Cambridge University Press, 1995).

[23] Deiglmayr, J., Grochola, A., Repp, M., Mörtlbauer, K., Glück, C., Lange, J., Dulieu, O., Wester, R., and Weidemüller, M., "Formation of Ultracold Polar Molecules in the Rovibrational Ground State," Physical Review Letters **101**, 133004 (2008).

[24] Deuretzbacher, F., Cremon, J. C., and Reimann, S. M., "Ground-state properties of few dipolar bosons in a quasi-one-dimensional harmonic trap," Physical Review A **81**, 063616 (2010).

[25] Duke, C. B., "Tunneling in Solids," in *Solid State Physics: Advances in Research and Applications*, supplement 10, edited by F. Seitz, D. Turnbull, and H. Ehrenreich (Academic Press, New York, 1969).

[26] Dzurak, A. S., Smith, C. G., Barnes, C. H. W., Pepper, M., Martín-Moreno, L., Liang, C. T., Ritchie, D. A., and Jones, G. A. C., "Thermoelectric signature of the excitation spectrum of a quantum dot," Physical Review B **55**, R10197 (1997).

[27] Dzurak, A. S., Smith, C. G., Pepper, M., Ritchie, D. A., Frost, J. E. F., Jones, G. A. C., and Hasko, D. G., "Observation of Coulomb blockade oscillations in the thermopower of a quantum dot," Solid State Communications **87**, 1145 (1993).

[28] Fahlvik Svensson, S., Burke, A. M., Carrad, D. J., Leijnse, M., Linke, H., and Micolich, A. P., "Using Polymer Electrolyte Gates to Set-and-Freeze Threshold Voltage and Local Potential in Nanowire-based Devices and Thermoelectrics," Advanced Functional Materials **25**, 255 (2015).

[29] Fahlvik Svensson, S., Jeppesen, S., Thelander, C., Samuelson, L., Linke, H., and Dick, K. A., "Control and understanding of kink formation in InAs–InP heterostructure nanowires," Nanotechnology **24**, 345601 (2013).

[30] Fahlvik Svensson, S., Persson, A. I., Hoffmann, E. A., Nakpathomkun, N., Nilsson, H. A., Xu, H. Q., Samuelson, L., and Linke, H., "Lineshape of the thermopower of quantum dots," New Journal of Physics **14**, 033041 (2012).

[31] Fasth, C., *Transport Studies of Local-Gate Defined Quantum Dots in Nanowires*, Ph.D. thesis, Lund University (2007).

[32] Fasth, C., Fuhrer, A., Björk, M. T., and Samuelson, L., "Tunable Double Quantum Dots in InAs Nanowires Defined by Local Gate Electrodes," Nano Letters **5**, 1487 (2005).

[33] Fasth, C., Fuhrer, A., Samuelson, L., Golovach, V. N., and Loss, D., "Direct Measurement of the Spin-Orbit Interaction in a Two-Electron InAs Nanowire Quantum Dot," Physical Review Letters **98**, 266801 (2007).

[34] Fetter, A. L. and Walecka, J. D., *Quantum Theory of Many-Particle Systems* (McGraw-Hill Book Company, 1971).

[35] Fuhrer, A., Fröberg, L. E., Pedersen, J. N., Larsson, M. W., Wacker, A., Pistol, M.-E., and Samuelson, L., "Few Electron Double Quantum Dots in InAs/InP Nanowire Heterostructures," Nano Letters **7**, 243 (2007).

[36] Gallagher, T. F. and Pillet, P., "Dipole-Dipole Interactions of Rydberg Atoms," Advances in Atomic, Molecular and Optical Physics **56**, 161 (2008).

[37] Ghosal, A., Güçlü, A. D., Umrigar, C. J., Ullmo, D., and Baranger, H. U., "Correlation induced inhomogeneity in circular quantum dots," Nature Physics **2**, 336 (2006).

[38] Ghosal, A., Güçlü, A. D., Umrigar, C. J., Ullmo, D., and Baranger, H. U., "Incipient Wigner localization in circular quantum dots," Physical Review B **76**, 085341 (2007).

[39] Giorgini, S., Pitaevskii, L. P., and Stringari, S., "Theory of ultracold atomic Fermi gases," Reviews of Modern Physics **80**, 1215 (2008).

[40] Gluschke, J. G., Svensson, S. F., Thelander, C., and Linke, H., "Fully tunable, non-invasive thermal biasing of gated nanostructures suitable for low-temperature studies," Nanotechnology **25**, 385704 (2014).

[41] Gross, E. K. U., Runge, E., and Heinonen, O., *Many-particle theory* (Institute of Physics Publishing, 1991).

[42] Guan, Q., Yin, X. Y., Gharashi, S. E., and Blume, D., "Energy spectrum of a harmonically trapped two-atom system with spin-orbit coupling," Journal of Physics B: Atomic, Molecular and Optical Physics **47**, 161001 (2014).

[43] Gurvitz, S. A. and Prager, Y. S., "Microscopic derivation of rate equations for quantum transport," **53**, 15932 (1996).

[44] Haake, F., "Statistical treatment of open systems by generalized master equations," in *Springer Tracts in Modern Physics*, edited by G. Höhler (Springer Berlin Heidelberg, 1973) pp. 98–168.

[45] Heremans, J. P., Dresselhaus, M. S., Bell, L. E., and Morelli, D. T., "When thermoelectrics reached the nanoscale," Nature Nanotechnology **8**, 471 (2013).

[46] Jackson, J. D., *Classical Electrodynamics*, 3rd ed. (John Wiley & Sons, New York, 1998).

[47] Kinaret, J. M., Meir, Y., Wingreen, N. S., Lee, P. A., and Wen, X.-G., "Many-body coherence effects in conduction through a quantum dot in the fractional quantum Hall regime," Physical Review B **46**, 4681 (1992).

[48] Kittel, C., *Introduction to Solid State Physics*, 8th ed. (Wiley, 2005).

[49] Koch, T., Lahaye, T., Metz, J., Fröhlich, B., Griesmaier, A., and Pfau, T., "Stabilizing a purely dipolar quantum gas against collapse," Nature Physics **4**, 218 (2008).

[50] Kubala, B. and König, J., "Quantum-fluctuation effects on the thermopower of a single-electron transistor," Physical Review B **73**, 195316 (2006).

[51] Lahaye, T., Koch, T., Fröhlich, B., Fattori, M., Metz, J., Griesmaier, A., Giovanazzi, S., and Pfau, T., "Strong dipolar effects in a quantum ferrofluid," Nature **448**, 672 (2007).

[52] Lahaye, T., Menotti, C., Santos, L., Lewenstein, M., and Pfau, T., "The physics of dipolar bosonic quantum gases," Reports on Progress in Physics **72**, 126401 (2009).

[53] Li, B., Slachmuylders, A. F., Partoens, B., Magnus, W., and Peeters, F. M., "Dielectric mismatch effect on shallow impurity states in a semiconductor nanowire," Phys. Rev. B **77**, 115335 (2008).

[54] Löw, R., Weimer, H., Nipper, J., Balewski, J. B., Butscher, B., Büchler, H. P., and Pfau, T., "An experimental and theoretical guide to strongly interacting Rydberg gases," Journal of Physics B: Atomic, Molecular and Optical Physics **45**, 113001 (2012).

[55] Lu, M., Burdick, N. Q., and Lev, B. L., "Quantum Degenerate Dipolar Fermi Gas," Physical Review Letters **108**, 215301 (2012).

[56] Movilla, J. L., Planelles, J., and Jaskólski, W., "From independent particles to Wigner localization in quantum dots: The effect of the dielectric environment," Physical Review B **73**, 035305 (2006).

[57] Nazarov, Y. V., "Quantum interference, tunnel junctions and resonant tunneling interferometer," Physica B **189**, 57 (1993).

[58] Ni, K.-K., Ospelkaus, S., de Miranda, M. H. G., Pe'er, A., Neyenhuis, B., Zirbel, J. J., Kotochigova, S., Julienne, P. S., Jin, D. S., and Ye, J., "A high phase-space-density gas of polar molecules." Science **322**, 231 (2008).

[59] Ni, K.-K., Ospelkaus, S., Wang, D., Quéméner, G., Neyenhuis, B., de Miranda, M. H. G., Bohn, J. L., Ye, J., and Jin, D. S., "Dipolar collisions of polar molecules in the quantum regime." Nature **464**, 1324 (2010).

[60] Nilsson, H. A., *Electron Tranport in Nanowire Quantum Devices*, Ph.D. thesis, Lund University (2010).

[61] Nilsson, H. A., Caroff, P., Thelander, C., Larsson, M., Wagner, J. B., Wernersson, L. E., Samuelson, L., and Xu, H. Q., "Giant, Level-Dependent g Factors in InSb Nanowire Quantum Dots," Nano Letters **9**, 3151 (2009).

[62] Olver, F. W. J., *Handbook of Mathematical Functions with Formulas, Graphs, and Mathematical Tables*, 10th ed., edited by M. Abramowitz and I. A. Stegun (Dover Publications, New York, 1972) Chap. 9.

[63] Ospelkaus, S., Ni, K.-K., Quéméner, G., Neyenhuis, B., Wang, D., de Miranda, M. H. G., Bohn, J. L., Ye, J., and Jin, D. S., "Controlling the Hyperfine State of Rovibronic Ground-State Polar Molecules," Physical Review Letters **104**, 030402 (2010).

[64] Pedersen, J. N. and Wacker, A., "Tunneling through nanosystems: Combining broadening with many-particle states," Physical Review B **72**, 195330 (2005).

[65] Reimann, S. and Manninen, M., "Electronic structure of quantum dots," Reviews of Modern Physics **74**, 1283 (2002).

[66] Reusch, B. and Egger, R., "Impurity effects in few-electron quantum dots: Incipient Wigner molecule regime," **84**, 84 (2003).

[67] Rontani, M., Cavazzoni, C., Bellucci, D., and Goldoni, G., "Full configuration interaction approach to the few-electron problem in artificial atoms," Journal of Chemical Physics **124**, 124102 (2006).

[68] Saarikoski, H., Reimann, S. M., Harju, A., and Manninen, M., "Vortices in quantum droplets: Analogies between boson and fermion systems," Reviews of Modern Physics **82**, 2785 (2010).

[69] Saffman, M., Walker, T. G., and Mø lmer, K., "Quantum information with Rydberg atoms," Reviews of Modern Physics **82**, 2313 (2010).

[70] Seebeck, T. J., "Ueber die magnetische Polarisation der Metalle und Erze durch Temperatur-Differenz," Annalen der Physik und Chemie **6**, 1 (1826).

[71] Serwane, F., Zuern, G., Lompe, T., Ottenstein, T. B., Wenz, A. N., and Jochim, S., "Deterministic Preparation of a Tunable Few-Fermion System," Science **332**, 336 (2011).

[72] Silvestrov, P. G. and Entin-Wohlman, O., "Wigner crystal of a two-dimensional electron gas with a strong spin-orbit interaction," Physical Review B **89**, 155103 (2014).

[73] Skinner, R. and Weil, J. A., "An introduction to generalized functions and their application to static electromagnetic point dipoles, including hyperfine interactions," American Journal of Physics **57**, 777 (1989).

[74] Slachmuylders, A. F., Partoens, B., Magnus, W., and Peeters, F. M., "Dielectric mismatch effect on the exciton states in cylindrical nanowires," Phys. Rev. B **74**, 235321 (2006).

[75] Turek, M. and Matveev, K., "Cotunneling thermopower of single electron transistors," Physical Review B **65**, 115332 (2002).

[76] Wacker, A., "Liouville approach with many-particle states," (2009), unpublished notes, version October 29, 2009.

[77] Wacker, A., "Different approaches to transport through quantum systems with interaction," (2011), unpublished notes, version January 29, 2011.

[78] Wang, J.-J., Li, W., Chen, S., Xianlong, G., Rontani, M., and Polini, M., "Absence of Wigner molecules in one-dimensional few-fermion systems with short-range interactions," Physical Review B **86**, 075110 (2012).

[79] Weis, J., "Single-Electron Devices," in *CFN Lectures on Functional Nanostructures Vol. 1*, Lecture Notes in Physics, Vol. 658, edited by K. Busch, A. Powell, C. Röthig, G. Schön, and J. Weissmüller (Springer Berlin Heidelberg, 2005) pp. 87–121.

[80] Wigner, E. P., "On the Interaction of Electrons in Metals," Physical Review **46**, 1002 (1934).

THE PAPERS

If I waited till I felt like writing, I'd never write at all.

Anne Tyler

I

PAPER I

SIGNATURES OF WIGNER LOCALIZATION IN EPITAXIALLY GROWN NANOWIRES

Líney Halla Kristinsdóttir[1], Jonas C. Cremon[1], Henrik A. Nilsson[2], Hongqi Xu[2], Lars Samuelson[2], Heiner Linke[2], Andreas Wacker[1], Stephanie M. Reimann[1]

[1]Division of Mathematical Physics, Lund University, Sweden
[2]Division of Solid State Physics, Lund University, Sweden

Physical Review B **83**, 041101(R) (2011) – Editor's choice
doi: 10.1103/PhysRevB.83.041101

II

PAPER II

TOTAL CURRENT BLOCKADE IN AN ULTRACOLD DIPOLAR QUANTUM WIRE

Líney Halla Kristinsdóttir[1], Olov Karlström[1], Johannes Bjerlin[1], Jonas C. Cremon[1], Peter Schlagheck[2], Andreas Wacker[1], Stephanie M. Reimann[1]

[1]Division of Mathematical Physics, Lund University, Sweden
[2]Département de Physique, Université de Liège, Belgium

Physical Review Letters **110**, 085303 (2013)
doi: 10.1103/PhysRevLett.110.085303

III

PAPER III

THERMOPOWER AS A TOOL TO INVESTIGATE MANY-BODY EFFECTS IN QUANTUM SYSTEMS

Líney Halla Kristinsdóttir[1], Jakob Bengtsson[1], Heiner Linke[2], Stephanie M. Reimann[1], Andreas Wacker[1]

[1]Division of Mathematical Physics, Lund University, Sweden
[2]Division of Solid State Physics, Lund University, Sweden

Applied Physics Letters **105**, 083105 (2014)
doi: 10.1063/1.4893928